Cell

LIS1 and NudE Induce a Persistent Dynein Force-Producing State

Richard J. McKenney,[1,4] Michael Vershinin,[2,4,6] Ambarish Kunwar,[3] Richard B. Vallee,[1,5,*] and Steven P. Gross[2,5,*]
[1]Department of Pathology and Cell Biology, Columbia University, New York, NY 10032, USA
[2]Department of Developmental and Cell Biology, University of California, Irvine, Irvine, CA 92697, USA
[3]Department of Neurobiology, Physiology & Behavior, University of California, Davis, Davis, CA 95616, USA
[4]These authors contributed equally to this work
[5]These authors contributed equally to this work
[6]Present address: Department of Physics, University of Utah, Salt Lake City, UT 84112, USA
*Correspondence: rv2025@columbia.edu (R.B.V.), sgross@uci.edu (S.P.G.)
DOI 10.1016/j.cell.2010.02.035

SUMMARY

Cytoplasmic dynein is responsible for many aspects of cellular and subcellular movement. LIS1, NudE, and NudEL are dynein interactors initially implicated in brain developmental disease but now known to be required in cell migration, nuclear, centrosomal, and microtubule transport, mitosis, and growth cone motility. Identification of a specific role for these proteins in cytoplasmic dynein motor regulation has remained elusive. We find that NudE stably recruits LIS1 to the dynein holoenzyme molecule, where LIS1 interacts with the motor domain during the pre-powerstroke state of the dynein crossbridge cycle. NudE abrogates dynein force production, whereas LIS1 alone or with NudE induces a persistent-force dynein state that improves ensemble function of multiple dyneins for transport under high-load conditions. These results likely explain the requirement for LIS1 and NudE in the transport of nuclei, centrosomes, chromosomes, and the microtubule cytoskeleton as well as the particular sensitivity of migrating neurons to reduced LIS1 expression.

INTRODUCTION

The major form of cytoplasmic dynein (dynein I; MAP1C) is involved in a wide range of cell movements, including vesicular and macromolecular transport, mitosis, and cell migration. The diversity of functions for this motor protein is matched by the complexity of its regulatory factors. LIS1 is a dynein-interacting protein encoded by the gene responsible for classical (type I) lissencephaly in humans (Reiner et al., 1993), a severe brain developmental disease. An ortholog of LIS1, *NudF*, was identified in a common "nuclear distribution" pathway with cytoplasmic dynein in *Aspergillus nidulans* (Xiang et al., 1995). An additional gene identified in the screen, *NudE,* has two mammalian counterparts, *Nde1* and *Ndel1* (protein names NudE and NudEL) (Efimov and Morris, 2000; Feng et al., 2000; Niethammer et al., 2000; Sasaki et al., 2000).

LIS1 and NudE/NudEL are now understood to have additional, more general functions in the cytoplasmic dynein pathway, including nuclear and centrosomal transport in migrating neurons (Shu et al., 2004; Tsai et al., 2005, Tsai et al., 2007), centrosome positioning in migrating nonneuronal cells (Dujardin et al., 2003; Shen et al., 2008; Stehman et al., 2007), growth cone advance (Grabham et al., 2007), chromosome alignment, and mitotic spindle orientation (Faulkner et al., 2000; Liang et al., 2007; Siller et al., 2005; Stehman et al., 2007; Vergnolle and Taylor, 2007).

The specific roles of LIS1, NudE, and NudEL in cytoplasmic dynein regulation are poorly understood. LIS1 associates with mitotic kinetochores via cytoplasmic dynein, rather than the reverse (Coquelle et al., 2002; Tai et al., 2002), suggesting that LIS1 is not employed in dynein recruitment to these structures. In contrast, NudE and NudEL can recruit both dynein and LIS1 to centrosomes and kinetochores (Guo et al., 2006; Stehman et al., 2007; Vergnolle and Taylor, 2007). LIS1, NudE, and NudEL interact physically with each other (Feng et al., 2000; Niethammer et al., 2000; Sasaki et al., 2000; Tarricone et al., 2004) and with the cytoplasmic dynein motor and cargo-binding domains (Sasaki et al., 2000; Stehman et al., 2007; Tai et al., 2002) and have been reported to have limited effects on dynein enzymatic activity (Mesngon et al., 2006; Yamada et al., 2008). LIS1 has also been reported either to stimulate (Sapir et al., 1997) or to suppress microtubule assembly (Han et al., 2001) and to interfere with dynein-mediated microtubule gliding (Yamada et al., 2008), but its effects on dynein at the single-molecule level are unknown.

In the current study, we used biochemical and biophysical approaches to investigate whether and how LIS1 and NudE might affect dynein motor activity. We find that NudE recruits LIS1 to the dynein molecule, and that, surprisingly, LIS1 binds to the dynein motor domain at the prepowerstoke stage in its crossbridge cycle. Using single-molecule measurements we find that NudE inhibits dynein force production. LIS1 alone or with NudE converts dynein to a sustained-force state and markedly enhances ensemble motor function for high load transport. These data provide insight into the molecular basis for

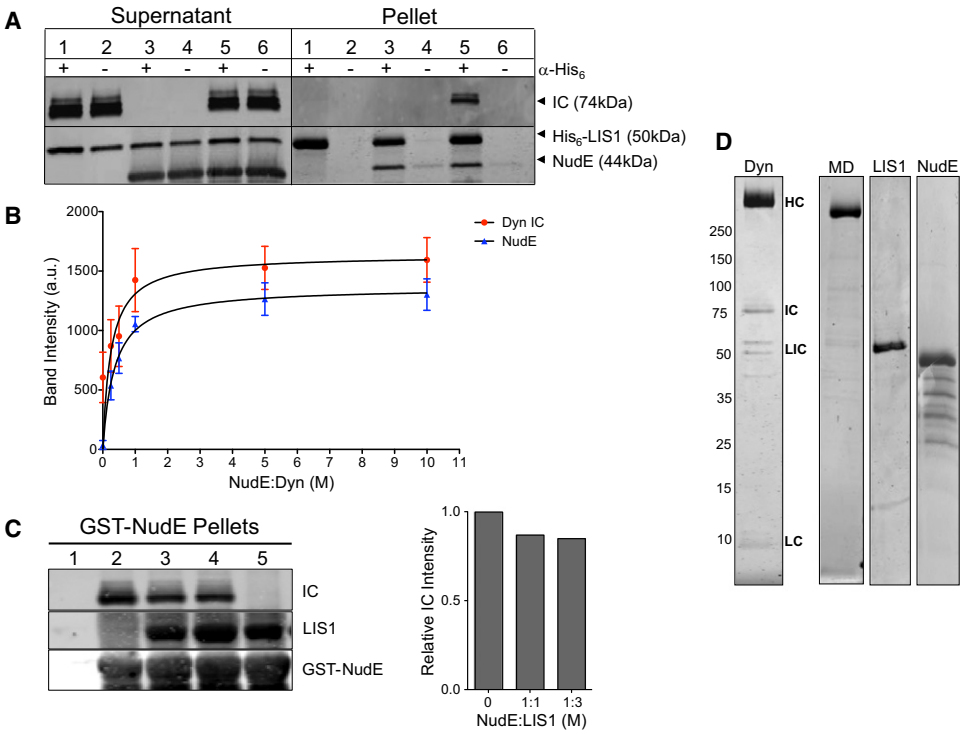

Figure 1. Dynein-NudE-LIS1 Interactions

(A) Recruitment of LIS1 to dynein by NudE. His_6-tagged LIS1 was immunoprecipitated with anti-His_6 antibody in the presence of purified brain dynein, NudE, or both. Immunoblotting shows no detectable coimmunoprecipitation of dynein (visualized by anti-intermediate chain [IC] antibody) with LIS1 (Pellet, lane 1) unless NudE is included (Pellet, lane 5).

(B) NudE concentration dependence of LIS1-dynein interaction. NudE was added in increasing amounts to a mixture of LIS1 and dynein, and the mixture was adsorbed to protein A beads coated with LIS1 antibodies. Quantitation of dynein (IC) and NudE pulled-down with LIS1 is shown. Dynein binding saturated at ~1:1 molar ratio with NudE. Mean of raw band intensity from four experiments is plotted in arbitrary units (a.u.) ± standard deviation (SD).

(C) LIS1 and dynein do not compete for NudE. GST-NudE-coated beads were mixed with dynein either in the absence of LIS1 (lane 2) or the presence of 1- (lane 3) or 3-fold (lane 4) molar stoichiometry of LIS1:NudE. The added LIS1 did not substantially affect the amount of dynein that bound to NudE, confirming that NudE can bind both LIS1 and dynein simultaneously (see Figure 7A). No proteins bound to beads without NudE (lane 1) and LIS1 could bind to NudE in the absence of dynein (lane 5). Right, quantification of the relative amount of dynein IC in the absence and presence of added LIS1 protein.

(D) Coomassie brilliant blue-stained gels of purified cytoplasmic dynein complex and recombinant proteins used in this study. MD: Purified dynein motor domain. Dynein subunits: HC—heavy chain; IC—intermediate chain; LIC—light intermediate chain; LC—light chain. Bands below NudE represent fragments, as judged by immunoblotting with anti-NudE antibody.

See also Figure S1.

lissencephaly and the mechanism of action of LIS1, NudE, and NudEL in a broad range of biological functions.

RESULTS

Cooperative, Nucleotide-Dependent LIS1, NudE, and Dynein Interactions

To define more completely the interactions between dynein and LIS1 or NudE, we used recombinant LIS1 and NudE and purified cytoplasmic dynein from calf brain (Paschal et al., 1987) using a method that includes a deaffinity step to specifically deplete kinesin motors as potential contaminants. The purified dynein holoenzyme (Figure 1D) is a complex of two 532 kDa heavy chains, the C-terminal 2/3 of which corresponds to the motor domains. The N-terminal dynein tail domains mediate dimerization and interactions with intermediate, light intermediate, and light chains. To examine dynein motor domain interactions specifically, we used a previously characterized 380 kDa baculovirus-expressed C-terminal dynein heavy chain fragment (Hook et al., 2005).

LIS1 coimmunoprecipitates with the cytoplasmic dynein holoenzyme complex (Faulkner et al., 2000; Smith et al., 2000) and with individual dynein subunits (Sasaki et al., 2000; Tai et al., 2002), but these interactions are relatively weak (Mesngon et al., 2006) (Figure 1A). Despite yeast two-hybrid and mammalian cell coexpression evidence for an interaction between LIS1 and the AAA1 ATPase portion of the dynein motor domain (Sasaki et al., 2000; Tai et al., 2002), we detect no cosedimentation of recombinant LIS1 with the purified 380 kDa baculovirus-expressed dynein motor domain (Figures 2A and 2B). To test whether this disparity could relate to changes in motor conformational states, we evaluated the effects of nucleotide and nucleotide analogs on the LIS1-motor domain interaction. We observed little or no interaction in the absence of nucleotide or

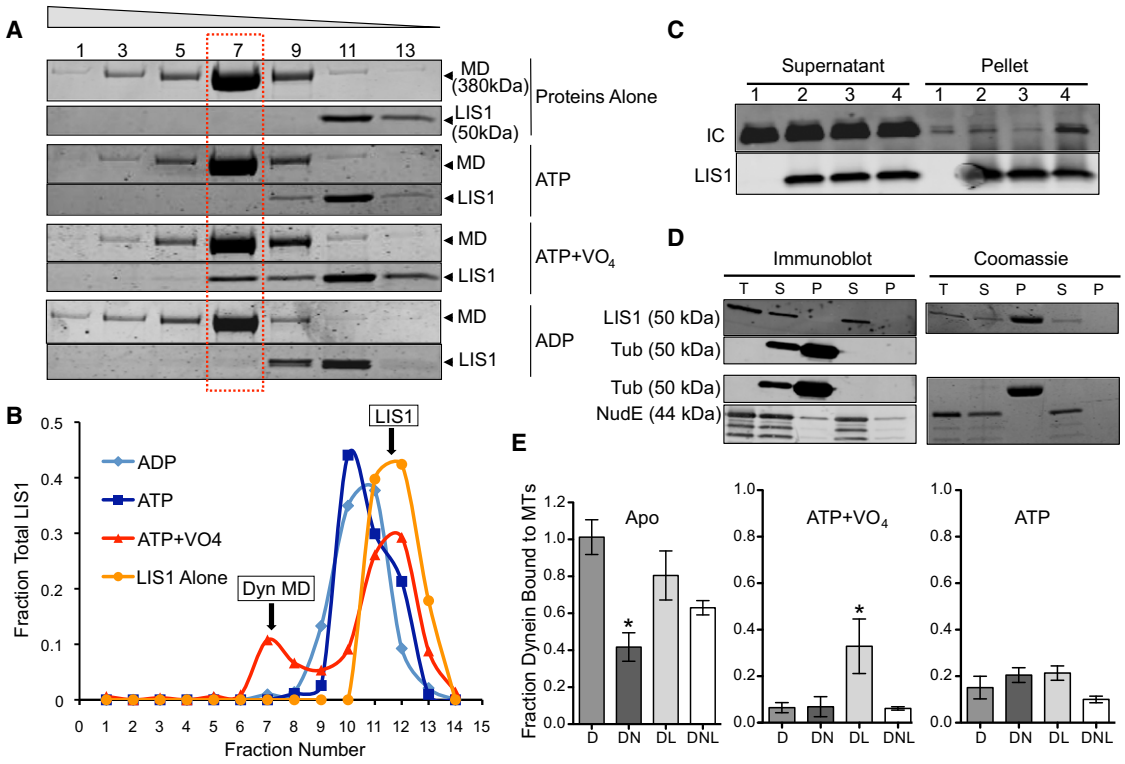

Figure 2. Effect of Nucleotides on Dynein-NudE-LIS1 Interactions

(A) Effect of nucleotides on LIS1 binding to dynein motor domain. Purified baculovirus-expressed dynein motor domain (MD) and LIS1 were incubated separately or together and sedimented through sucrose gradients containing the indicated nucleotides. Coomassie brilliant blue-stained gels show a fraction of LIS1 to cosediment with the purified dynein motor domain peak (dashed box) in the presence of ATP and VO_4 but not ATP alone or ADP. Sucrose concentration and fraction numbers are indicated at top.

(B) Quantitation of LIS1 distribution showing a major low s value peak for the free protein and, in the ATP+VO_4 condition, a smaller peak cosedimenting with the dynein motor domain.

(C) Effect of nucleotides on LIS1 binding to purified calf brain dynein. Dynein was incubated with beads alone (lane 1) or LIS1-coated beads in the absence of nucleotide (lane 2) or in the presence of ATP (lane 3) or ATP+VO_4 (lane 4). Dynein (IC) is enriched in the LIS1 pellet only in the ATP+VO_4 condition.

(D) LIS1 and NudE do not bind to microtubules. Purified LIS1 and NudE were sedimented in the presence or absence of microtubules. Total protein (T), supernatants (S) and pellets (P) are shown by immunoblotting and Coomassie blue staining. LIS1 is obscured by tubulin in the Coomassie blue-stained gel, but immunoblotting shows LIS1 not to sediment with microtubules. NudE also shows no evidence of microtubule cosedimentation.

(E) Effect of LIS1 and NudE on dynein binding to microtubules. Purified brain dynein was mixed with microtubules in the absence of nucleotide (Apo) or in the presence of ATP or ATP+VO_4, and the microtubules were sedimented. NudE strongly inhibited binding of dynein to microtubules in the apo state (DN; *p = 0.0011, two-tailed t test), an effect partially rescued by LIS1 (DNL). Conversely, LIS1 increased dynein binding to microtubules in the ATP+VO_4 state by approximately 5-fold (DL; *p = 0.0131, two-tailed t test). Error bars represent mean ± SD of three experiments.

in the presence of ATP, AMPPNP (not shown), or ADP but a clear interaction in the presence of ATP plus sodium vanadate (VO_4), as indicated by a shift in LIS1 to the dynein motor domain peak (molar ratio dynein motor:LIS1 dimer = 1.3; Figures 2A and 2B). A similar, nucleotide-dependent interaction is seen between LIS1 and the purified brain dynein (Figure 2C). ATP hydrolysis in the presence of VO_4 leads to a dynein-ADP-VO_4 dead-end complex, which is thought to mimic the prepower stroke transition state (Shimizu and Johnson, 1983), strikingly revealed by electron microscopy (Burgess et al., 2003). Our results suggest, therefore, that LIS1 interacts with the dynein motor domain at a specific, transient stage in its enzymatic cycle. The interaction site within the motor domain remains to be explored further but could involve AAA1 (Sasaki et al., 2000; Tai et al., 2002).

NudEL has been reported to interact with the dynein motor domain on the basis of yeast two-hybrid analysis (Sasaki et al., 2000). We detect no interaction between recombinant NudE and dynein motor domain under any nucleotide condition (Figure S1B available online) but have, instead, observed a clear interaction between NudE and the intact cytoplasmic dynein complex mediated through the intermediate and light chains located in the base of the dynein molecule (Stehman et al., 2007). NudE and NudEL bind through an unstructured C-terminal domain to dynein, and to LIS1 through a distinct N-terminal coiled-coil domain (Derewenda et al., 2007; Liang et al., 2004; Sasaki et al., 2000; Tarricone et al., 2004; Yan et al., 2003), leading us to speculate that NudE or NudEL might act to link LIS1 to dynein (Figure 7). Indeed, in the absence of nucleotide, the ability of LIS1 to pull down purified calf brain dynein was

completely dependent on addition of NudE (Figures 1A and 1B). The interaction showed a clear NudE concentration dependence and appeared to saturate at a molar stoichiometry of ~1:1 NudE:dynein (Figure 1B). LIS1 and dynein showed no evidence of competition for NudE binding (Figure 1C). Together, our results indicate that LIS1 alone interacts transiently with the dynein motor domain, but that NudE tethers LIS1 to dynein to form a more stable tripartite complex.

We also examined the effects of LIS1 and NudE on dynein-microtubule interactions. Alone, neither LIS1 nor NudE bound microtubules (Figure 2D). LIS1 had little effect on dynein-microtubule binding in the apo or ATP state (Figure 2E) but increased binding 5.1-fold in the presence of ADP-VO_4 (Figure 2E). This increase is intriguing because dynein binds weakly to microtubules in this condition (Imamula et al., 2007; Shimizu and Johnson, 1983). Thus, our data suggest that LIS1 increases the affinity of dynein for microtubules specifically during the prepowerstroke stage of the crossbridge cycle.

In contrast, NudE decreased dynein-microtubule binding by 60% in the absence of nucleotide, which corresponds to the strong binding (apo) state of the dynein mechanochemical cycle (Figure 2E). Little further effect on dynein-microtubule binding was observed in the presence of ATP or ATP plus VO_4 (Figure 2E).

LIS1 had no effect on basal or microtubule-stimulated dynein ATPase activity in our assays (Figure S1A), in contrast to one report (Mesngon et al., 2006) but consistent with another (Yamada et al., 2008). However, the microtubule-stimulated component of dynein ATPase activity was inhibited 50% by addition of NudE alone and by 72% with further addition of LIS1 (Figure S1A).

Effect of LIS1 on Dynein Behavior in Single-Molecule Assays

To determine the effects of LIS1 and NudE on the behavior of individual dynein molecules directly, we adsorbed dynein to carboxylated polystyrene beads and monitored transport and force production according to established methods (Gennerich et al., 2007; Mallik et al., 2004; Vershinin et al., 2008). Dynein was applied at dilutions at which ≤30% of beads bound to microtubules (bead-binding fraction ≤0.3) to ensure predominantly single-motor events (Svoboda and Block, 1994). In the absence of applied force, dynein induced bead translocation at ~1 μm/s (Figure 3), within the range of previous reports (King and Schroer, 2000; Mallik et al., 2005; Paschal and Vallee, 1987; Ross et al., 2006) but ~10-fold faster than recombinant yeast cytoplasmic dynein (Reck-Peterson et al., 2006). Some bidirectional motion was observed, as previously reported (Gennerich et al., 2007; Mallik et al., 2005; Ross et al., 2006). Moderate levels of LIS1 did not affect processivity (Figure 3A), but net bead velocity was somewhat reduced due to increased bead pausing. Discrete pauses were infrequent at 1:1 LIS1:dynein but increased with LIS1 concentration (Figure 3C; note extreme example in Figure S3).

To test for effects of LIS1 on dynein force production, optical trapping was employed at single dynein molecule levels. The dynein beads showed clear evidence of force production, as previously described (Gennerich et al., 2007; Mallik et al., 2004; Reck-Peterson et al., 2006; Toba et al., 2006), with a stall force

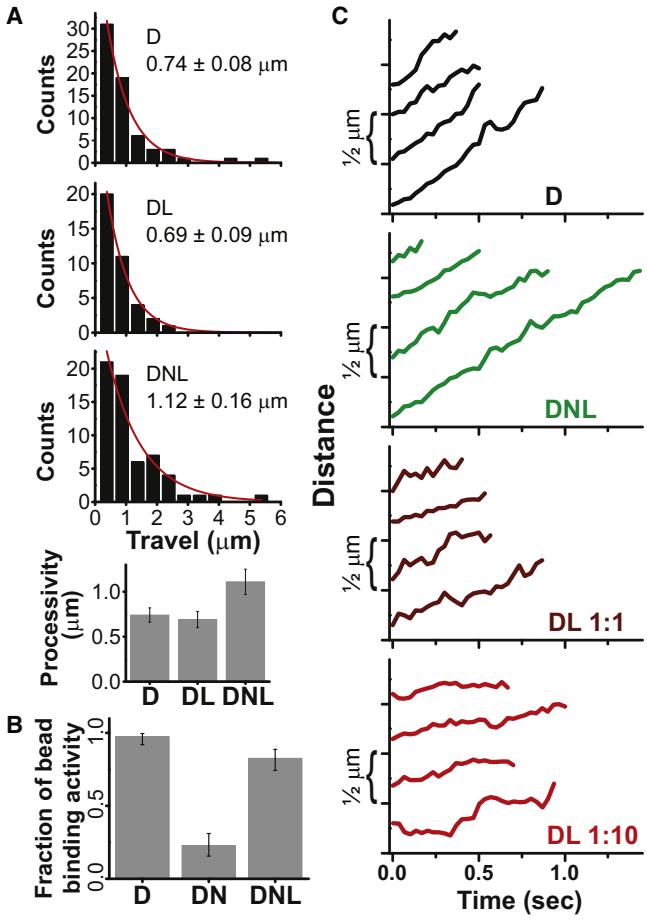

Figure 3. Effect of LIS1 and NudE on Dynein Motility

(A) Histogram of single dynein travel distances alone (D), in the presence of LIS1 (molar ratio of D:L = 1:2), and in the presence of both NudE and LIS1 (D:N:L = 1:9:10). Exponential decay fits are shown in red, and decay constant ± standard error of the mean (SEM) is indicated in each case. A small percentage of beads had bidirectional motion of 2 μm or more in each direction, did not spontaneously detach from microtubules, and were excluded from analysis; such beads showed no force production capacity in either direction and were deemed to be diffusive rather than processive. D and DL processivity values are similar, whereas DNL processivity is clearly increased ($p < 0.03$).

(B) Microtubule-binding activity for D, DN, and DNL beads. We quantify the percentage of beads with visible binding and travel events, held close to a microtubule in a weak optical trap (See Experimental Procedures). NudE (molar ratio 1:9 D:N) potently reduced microtubule-binding activity, an effect rescued by addition of LIS1 (D:N:L= 1:9:2). Neither LIS1 nor NudE produced a comparable inhibition of binding activity in similar experiments with kinesin motors (Figure S2B). Exact CI error bars are reported (see Supplemental Information).

(C) Individual traces of motor-driven movements along microtubules (D:L ratios indicated; D:N:L is as in A). D (black) and DNL (green) beads show robust motility whereas DL bead movements (dark and light red) are interrupted by pauses that result in a net slow-down of transport. The effect becomes more prominent as the LIS1 concentration increases. See Figure S3 for more extended and extreme examples of bead travel. For all experiments, dynein was first adsorbed to beads, followed as needed by NudE and then by LIS1.

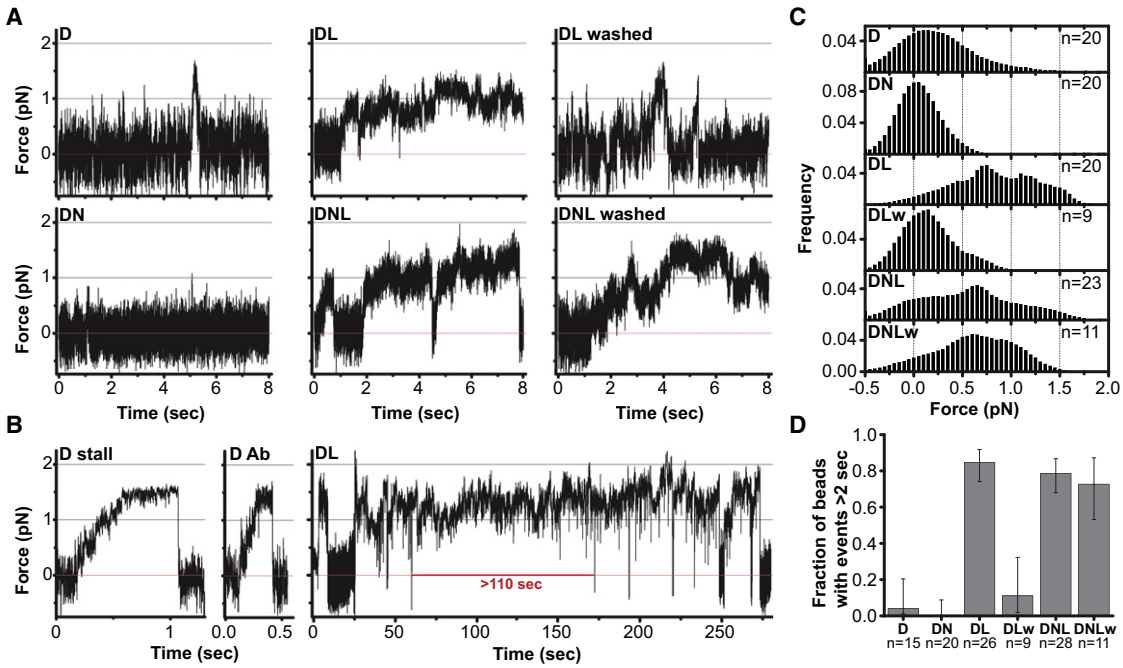

Figure 4. The Effect of NudE and LIS1 on Dynein Force Production

(A) Representative records of single-motor force production in an optical trap for beads with bound dynein (D); dynein + NudE (DN); dynein + LIS1 (DL); and dynein + NudE + LIS1 (DNL). Red line marks center of optical trap. Dynein beads (D) typically detach before the motor can stall, but short (~0.5 s) stalls occasionally occur (see B). DN beads (1:9 D:N) show almost no motion. However, DL and DNL beads (1:2 D:L and 1:9:2 D:N:L) exhibit dramatically longer force production events, some of which continue beyond the period shown (and see panel B). Similar behavior under load was also observed at higher amounts of LIS1 (1:10 D:L) in DL and DNL assays (see Figure S4). The prolonged dynein stalls induced by LIS1 were eliminated by washing the beads (see Experimental Procedures) in the DL assay (DL washed) but not the DNL assay (DNL washed). These observations support our biochemical results indicating that NudE retains LIS1 in a complex with dynein (Figures 1A and 1B).

(B) Representative stalls for dynein adsorbed to beads nonspecifically (D stall) or through anti-dynein IC monoclonal antibody (D Ab) illustrate maximal force production for single dynein motors. (DL) An extremely long (~110 s) event (entire tracing is shown) demonstrating dramatic prolongation of dynein force production by LIS1.

(C) Distribution of forces attained during prominent bead-microtubule binding events sampled in a 4 s window and summed from multiple bead assays (n = 9–23 as indicated). DN shows minimal bead displacement almost symmetrically distributed around the trap center, indicating that bead motion is predominantly due to thermal noise. D alone exhibits a shift to higher forces. The shift is dramatically greater for DL and DNL, indicating higher average force production. Notably, this effect was retained when DNL beads were washed to remove excess proteins from solution (DNLw) but abolished when DL beads were similarly washed (DLw). This suggests that DNL association is stable but the DL one is not.

(D) The fraction of beads exhibiting long force production events (>2 s) is dramatically increased in the presence of LIS1. The effect is again abolished in DL-washed (DLw) but not in DNL-washed (DNLw) assays. Exact CI error bars are reported (see Supplemental Information).

See also Figure S4.

of 1.0–1.5 pN (Mallik et al., 2004; Schroeder et al., 2008; Figures 4A and 4B). Comparable values were obtained with dynein bound directly to beads or through an anti-dynein intermediate chain antibody (1.4 ± 0.2 pN, n = 11; Figure 4B, "D Ab") and for chicken and mouse cytoplasmic dynein (1.3–1.4 pN, J. Xu and K. Ori-McKenney, personal communication). Another vertebrate dynein preparation has been reported with a higher stall force when adsorbed nonspecifically to protein A-coated beads, but with differences in several additional properties (Toba et al., 2006). Yeast cytoplasmic dynein has also been reported to have a higher stall force (Reck-Peterson et al., 2006), but its 10-fold slower transport rate and C-terminally truncated motor domains suggest a phylogenetic basis for its differences from mammalian cytoplasmic dynein.

As reported (Mallik et al., 2004), clean dynein stalling events could be detected in the optical trap (Figure 4B, panel "D stall"; Figure S4, top), but, more typically, dynein detached before reaching its full stall load (Figure 4A, panel "D"). The maximum duration of dynein stalls was ~2 s, as reported (Mallik et al., 2004). In marked contrast, addition of LIS1 induced periods of dramatically sustained load-bearing events (Figure 4). These persistent "stall-like events" lasted from several seconds to >100 s in the longest case. Periods of sequential stall-like events with only transient interruptions were also common and lasted up to 250 s (Figure 4B, "DL," additional examples Figure S4). Analysis of combined tracings from multiple beads revealed that, in the presence of LIS1, dynein beads spent much more time at higher average forces (Figure 4C, panels D versus DL).

These effects reflect LIS1-induced alteration of dynein behavior based on several considerations. LIS1 showed no microtubule binding on its own (see above, Figure 2D), nor did LIS1-coated beads bind microtubules (Figure S1). The LIS1

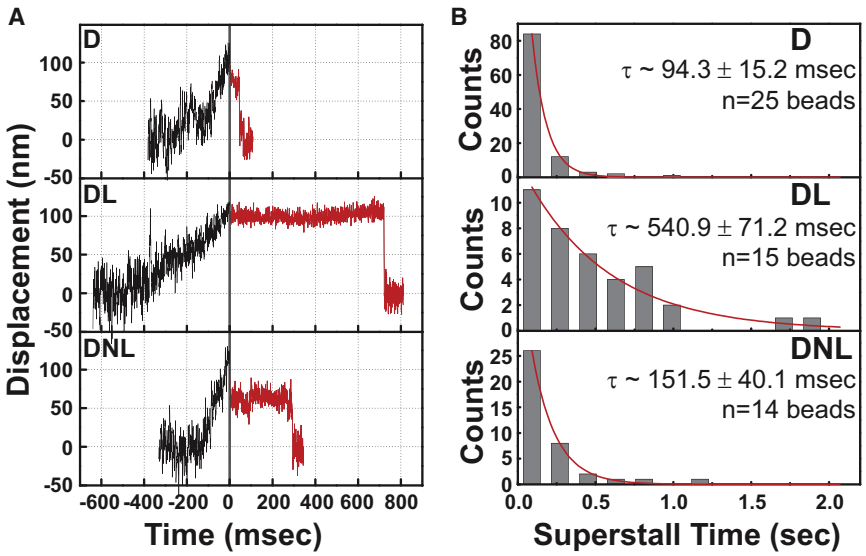

Figure 5. LIS1 Enhances Dynein-Microtubule Interaction under Load

(A) Beads driven by single dynein motors were allowed to move along microtubules in a weak optical trap (black traces). At 100 nm bead displacement from the trap center, laser power was automatically increased (T = 0, solid vertical line), subjecting dynein to a load of ~2 pN, significantly greater than the dynein stall force ("superstall" conditions). Subsequent bead positions are shown as red lines and demonstrate prolonged persistence of DL bead (1:10 D:L) on microtubule and less so of DNL (1:9:10 D:N:L) bead.

(B) Analysis of multiple superstall traces as in (A) revealed that average detachment times in both DL and DNL assays were significantly increased relative to D alone. Exponential decay constant ± SEM is shown in each subpanel.

effect on dynein could be eliminated by preincubation of the his-tagged LIS1 with Ni^{2+}-NTA beads (data not shown) and specifically retained by NudE in bead-washing experiments (see below). Finally, LIS1 showed no biochemical interaction with kinesin, nor did it affect kinesin-mediated bead transport or the duration of kinesin stalls (Figure S2).

Effects of NudE and NudE Plus LIS1 on Dynein Behavior in Single-Molecule Assays

In contrast to LIS1, and consistent with its effect on dynein microtubule binding (Figure 2E), NudE reduced the frequency of microtubule-binding events by dynein beads (Figure 3B). Bead travel in the presence of NudE was typically below the level of noise-driven fluctuations (~25–40 nm; Figure 4A, "DN"). Because of the minimal bead binding in the presence of NudE, the optical trap was needed to hold beads in proximity to microtubules. The overall effect of NudE was a dramatic reduction in dynein-mediated force production (Figure 4C, "DN"). As for LIS1, and consistent with our biochemical analysis (Figure 2D), beads coated with NudE alone showed no microtubule-binding activity (Figure S1 and Figure 2D). Furthermore, NudE showed no binding to kinesin and had little effect on the ability of kinesin beads to bind microtubules or produce force (Figure S2).

To test the combined effects of LIS1 and NudE, we exposed beads to dynein, followed by NudE and LIS1 (see Experimental Procedures). LIS1 rescued the dramatic inhibition of bead-microtubule interactions observed with NudE alone (Figure 3B). Conversely, NudE completely eliminated LIS1-induced bead pausing (Figure 3C), as indicated by visual inspection of bead traces and by restoration of average bead velocity (D = 1.05 ± 0.12; DL at 1:10 = 0.23 ± 0.04; DNL at 1:10:10 = 1.04 ± 0.06). In addition, LIS1 plus NudE significantly increased dynein bead processivity relative to dynein-coated beads alone (Figures 3A and 3C). Most significantly, NudE and LIS1 together dramatically increased the duration of dynein stall-like events (Figure 4 and Figure S4), but with maximal force levels unchanged.

Our biochemical analysis indicated that NudE mediates the interaction between dynein and LIS1. To test whether NudE recruits LIS1 to dynein in the bead assay, we adsorbed dynein at single-molecule concentrations, followed by LIS1 alone or LIS1 with NudE. We then removed excess proteins by centrifugation and resuspension of the beads in motility buffer alone. For beads exposed to dynein and LIS1, the effect of LIS1 was markedly reduced by washing. For beads exposed to dynein, LIS1, and NudE and then washed, clear preservation of sustained force events was observed (Figure 4, DL versus DL washed; and DL washed versus DNL washed). We conclude that NudE, indeed, stabilizes the LIS1-dynein interaction in these assays.

Direct Analysis of LIS1-Modulated Dynein Detachment from Microtubules under Load

Pull-off experiments (Evans, 2001) assay the strength of protein-protein interactions directly with high temporal and spatial resolution and were used to measure dynein's affinity for microtubules with or without LIS1 and NudE. When trapped beads had moved ~100 nm from the trap center, laser intensity was doubled to exceed the dynein stall force ("superforce"). Typically, after very brief pauses, dynein beads detached from the microtubule and returned rapidly toward the trap center with a $t_{1/2}$ = 94.2 ms (Figures 5A and 5B). In the presence of LIS1, dynein beads remained attached up to 1–2 s ($t_{1/2}$ = 540.9 ms; Figures 5A and 5B, panels "DL"). LIS1 and NudE combined also increased the duration of binding relative to dynein alone, though less substantially. Thus, LIS1 allows dynein to remain bound longer under load, indicating that LIS1 increases the effective strength of the dynein-microtubule interaction.

Effects of NudE and LIS1 on Dynein Behavior in Multiple-Motor Assays

How multiple motors function together to achieve active transport is only partially understood. To explore how LIS1 and NudE affect the behavior of multiple dynein motors, we conducted

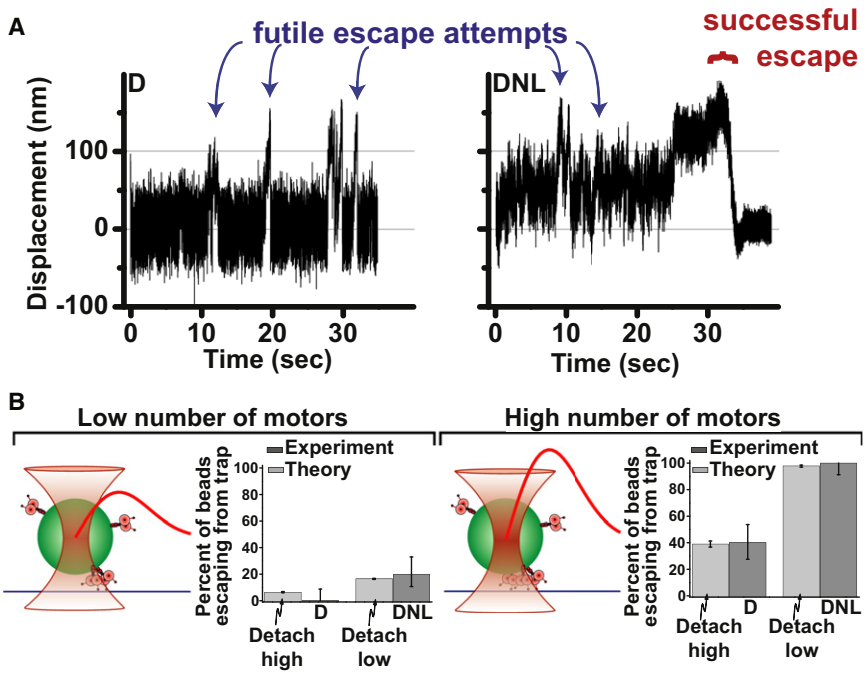

Figure 6. LIS1 and NudE Enhance Multiple-Motor Function

To test the effect of NudE and LIS1 on multiple dynein motors, beads were incubated with concentrations of dynein above those used for single-molecule experiments.

(A) Force records from individual beads exposed to dynein (D) or the same amount of dynein followed by NudE and LIS1 (DNL). High force events can be observed (blue arrows), as can bead escapes from trap confinement (red bracket).

(B) Quantification of trap escape. The fraction of high force events resulting in escape was scored for D versus DNL at low (left) and high (right) concentrations of applied dynein (dark gray bars, n = 20 in each case). Maximum trap force was estimated at 1.8 pN and 3.7 pN for these two assays, respectively (therefore, synergistic activity of $\geq$2 and $\geq$3 motors was required for a successful escape event to occur in these two assays, respectively). The frequency of trap escapes was clearly increased in DNL versus D alone. Theoretical modeling (light gray bars) conservatively assuming a 50% change of time to detachment for each dynein motor (*cf* Figure 5B) is predicted to be sufficient to account for the observed difference between D and DNL escape frequencies (see Extended Experimental Procedures). Schematic diagram of the experiment (left of each histogram): the bead (green) with motors attached to its surface (rose) is held near a microtubule (blue) by an optical trap (hyperboloid shape). Trap strength (red curve) rises approximately linearly as the distance from trap center grows, then saturates and finally decays to zero. Exact CI error bars are reported (see Extended Experimental Procedures). See also Figure S5.

"trap escape" assays using beads incubated with increased concentrations of dynein. Force production was monitored for two different force/motor-number combinations, using either a 1.8 pN escape force (requiring two motors to escape, Figure 6B, left) or a 3.7 pN escape optical trap (sufficient to prevent two but not three dynein motors from escaping, Figure 6B, right). The addition of LIS1 and NudE caused a significant increase in the number of beads able to escape from the optical trap along microtubules (Figures 6A and 6B), consistent with a dramatic improvement in multiple-motor performance.

To determine whether the large improvement in multiple-motor performance could be explained by the LIS1-induced decreased detachment rate under load, we modeled single dynein motor activity using a Monte-Carlo approach used for kinesin (Kunwar et al., 2008) but reflecting unique features of dynein motility (most notably non-negligible back-stepping probability even under zero load). Importantly, modeling was highly constrained by experimental data, especially microtubule dissociation rate and stall force (this study) and back-stepping rate (Mallik et al., 2005). Dynein motility modeled in this way was similar to the experimentally observed records (Figure S5A). We then expanded the single dynein model to simulate two or more motors functioning together to match each of the two experimental conditions (Figure 6) for motor ensemble performance under load. Thus, motor number was adjusted in the simulation until the correct proportion of dynein-only beads escaped from the trap (Figure 6B, bars labeled "detach high"). The simulations for the dynein-NudE-LIS1 case were then performed identically, except for the change in individual motor detachment rate under load (Figure 5). This theoretical change in single-molecule properties indeed yielded a predicted change in ensemble motor function, so that the resulting frequency of high-force motility events was very comparable to the trap escape frequency we observed experimentally due to addition of NudE and LIS1 (Figure 6B, bars labeled "detach low," Figure S5B), with no additional adjustments or free parameters required. Thus, the modeling suggests that the improved multiple-motor behavior observed experimentally can be entirely explained by the measured cofactor-induced changes in single-molecule function. Technical details of the theoretical modeling are provided in the Experimental Procedures and the Extended Experimental Procedures.

DISCUSSION

LIS1, cytoplasmic dynein, NudE, and NudEL have long been known to function in a common genetic pathway. The mechanistic implications of the interactions among these proteins have remained a major question in the field of developmental neuroscience, motor protein research, and cell biology. NudE and NudEL have been implicated in some aspects of dynein recruitment to subcellular sites, but this has not been the case for LIS1, and its functions as well as how its activity may be modulated by NudE and NudEL have remained largely unknown.

LIS1 is essential for neuronal migration, based on the altered distribution of neurons in the lissencephalic brain (Dobyns, 1987; Hirotsune et al., 1998; Reiner et al., 1993) and direct imaging of migrating neurons in fixed (Shu et al., 2004) and live

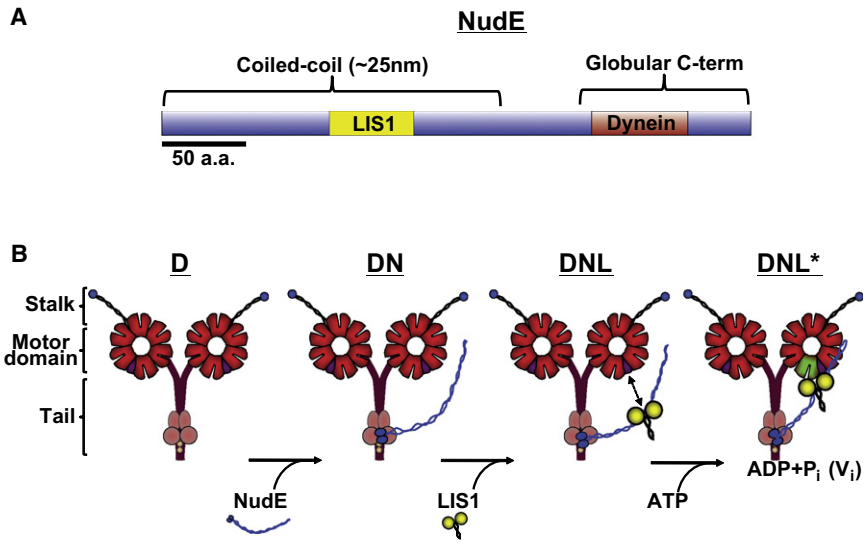

Figure 7. Diagrammatic Representation of Dynein-LIS1-NudE Interactions and Functional Consequences

(A) Bar diagram of NudE shows coiled-coil and unstructured C-terminal domains and known LIS1- and dynein-binding regions (see text for details).

(B) Proposed assembly intermediates in dynein-NudE-LIS1 complex. Known binding of NudE to dynein intermediate and light chains (Stehman et al., 2007) predicts an association of the NudE C terminus with the base of the dynein molecule, with its coiled-coil domain postulated to protrude as shown. The calculated distance between the NudE-dynein site and the known LIS1-binding site in the middle of the NudE coiled-coil α-helical tail (Derewenda et al., 2007) is proposed here to be sufficient to allow NudE to position LIS1 near the dynein motor domains. LIS1 is shown unbound to the dynein motor domain as we observe under most conditions but is proposed to bind specifically in the ADP-VO_4 prepowerstroke state (Figure 2).

embryonic brain tissue (Tsai et al., 2005). No other dynein-related effects have been reported to be altered in humans with LIS1 mutations or in mouse models. LIS1 dominant-negative cDNAs had potent effects on cell migration and division, but not on other dynein functions such as Golgi, endosome, and lysosome positioning (Faulkner et al., 2000, though see Smith et al., 2000). LIS1 may, thus, contribute to a subset of cytoplasmic dynein functions, but the nature of its specific role has been obscure. Here we identify LIS1 and NudE as regulators of dynein force production, the first such proteins implicated in this role. How this behavior relates to the biological functions of LIS1 is discussed below.

LIS1-NudE-Dynein Complex

Despite prior evidence for a LIS1-dynein motor domain interaction (Sasaki et al., 2000; Tai et al., 2002), it must be very weak or transient in view of the lack of binding we typically observe between the purified components (Figure 1D). We find, however, that NudE can mediate LIS1 binding to the dynein complex in an efficient, saturable, and apparently stoichiometric manner (Figures 1A, 1B, and 7). Consistent with this conclusion, NudE retained LIS1 on dynein beads washed to remove free protein (Figures 4A, 4C, and 4D).

Our data provide evidence for a triple complex of LIS1, NudE, and cytoplasmic dynein, with a potential structural arrangement as shown in Figure 7B. NudE and NudEL interact via an unstructured C-terminal domain with the dynein intermediate and light chains (Stehman et al., 2007) at the base of the dynein molecule (Figure 7B). LIS1, in contrast, interacts within the N-terminal coiled-coil region of NudE and NudEL (amino acids 103–153 and 102–152, respectively) (Derewenda et al., 2007; Sasaki et al., 2000) (Figure 7B). The LIS1 site, therefore, can be estimated to lie approximately 15 nm from the C terminus of NudE. As depicted in Figure 7B, association of NudE with the intermediate and light chains at the base of the dynein molecule could, therefore, place LIS1 close to the motor domains. Whether NudE and LIS1 are oriented in this manner is unknown. However, our biochemical and biophysical evidence that LIS1 linked to dynein through NudE remains capable of altering dynein motor function makes this an appealing speculation.

We suggest, therefore, that NudE and NudEL serve in communication between the dynein tail and motor domains. Nonmuscle myosin II isoforms, myosin V, and some kinesins each exhibit such a mechanism, but through direct intramolecular interactions between tail and motor domains (Dietrich et al., 2008; Krementsov et al., 2004; Scholey et al., 1980; Stock et al., 1999; Wang et al., 2004). Such a feature is as yet unknown for cytoplasmic dynein. Our results suggest that NudE and/or NudEL could play such a role, though as the first extramolecular factors with such a function.

Effects of LIS1 and NudE on Dynein Motor Activity

We find LIS1 and NudE each to have dramatic effect on cytoplasmic dynein motor activity in our single-molecule assays. LIS1 prolonged dynein force-producing events, often for substantial periods of time. LIS1 likely acts at a precise stage in the dynein crossbridge cycle, as it bound to the dynein motor domain only in the presence of ATP plus VO_4 (Figure 2A), which arrests dynein at the prepowerstroke state. LIS1 also caused a 5-fold enhancement of dynein binding to microtubules under these conditions (Figure 2E), suggesting a specific increase in microtubule affinity in the prepowerstroke stage. Single-molecule superforce experiments (Figure 5) showed a decreased rate of dynein dissociation from microtubules under load, consistent with increased affinity (Gebhardt et al., 2006; Veigel et al., 2005). Together, our results reveal that LIS1 prolongs the interaction of dynein with microtubules, specifically during the prepowerstroke and possibly the powerstroke states. A similar transition state-specific interaction involving the bacterial enhancer-binding protein (EBP), another member of the AAA+ protein family, was recently reported (Chen et al., 2007), suggesting that transition state interactions may be an evolutionarily conserved mechanism in this extended protein superfamily.

NudE affected dynein behavior in a manner opposite from LIS1, but apparently at a different stage of the dynein crossbridge cycle, corresponding to the apo state. We observed no

binding of NudE to the dynein motor domain under any nucleotide condition (Figure S1B), in contrast to LIS1. However, NudE strongly decreased the ability of the purified brain dynein complex to bind to microtubules, and, in bead assays, single dynein-microtubule interactions were almost eliminated. Whether this potent NudE inhibition results from steric hindrance of the motor-microtubule interaction or more direct regulation of motor activity is uncertain. We do not confirm a previously reported weak interaction between NudEL and fragments of the dynein motor domain (Sasaki et al., 2000). This may be a result of the use of the complete motor domain in the current study, which we find to be physically and enzymatically very well behaved (Hook et al., 2005).

The combination of LIS1, dynein, and NudE produces what appears to be a streamlined molecular machine converted to function in sustained force production. The LIS1-induced pauses observed in freely moving beads are eliminated by the addition of NudE, and dynein processivity is increased, while prolongation of force-producing events persists. Furthermore, the concentration of LIS1 required for this effect appears to be greatly reduced, as the ability to induce prolonged force events persists following bead washing (Figures 4A and 4C). We hypothesize that these results reflect retention of LIS1 to dynein in the presence of NudE. In addition, we hypothesize that LIS1 is stereospecifically positioned by NudE for greater efficiency of dynein force regulation (Figure 7B).

We observed clear inhibition of microtubule-stimulated dynein ATPase activity by NudE alone and NudE plus LIS1 (Figure S1A), though we saw little effect of LIS1 alone. This result may simply reflect the preferential effect of LIS1 on dynein under load. It is also possible that dynein ATP hydrolysis persists during the stalled state, either from activity at the principal ATPase site, AAA1, or at the subsidiary sites (Kon et al., 2004). ATPase and microtubule-binding activity can be uncoupled in dynein stalk mutants (Kon et al., 2009), and it is conceivable that LIS1 could contribute to comparable effects. An earlier study also found little effect of LIS1 on dynein ATPase activity (Yamada et al., 2008), though another study found a modest ~40% stimulation (Mesngon et al., 2006). Further research will be needed to clarify what effects LIS1 may have on the complex dynein ATPase cycle.

Biological Implications

Our data have important biological implications. LIS1 is required for cytoplasmic dynein activities that appear to involve very high load, including transport of, or tension on, nuclei, chromosomes, and even the entire microtubule cytoskeleton (Grabham et al., 2007; Tsai et al., 2007). Nuclei, in particular, show signs of extreme distortion as they attempt to advance within migrating neurons against great resistance (Tsai et al., 2007). This resistance is overcome by LIS1 and dynein in control cells, but it is blocked by LIS1 or dynein RNAi (Tsai et al., 2007). By conferring on dynein the ability to resist release from microtubules under load, we envision that LIS1 permits the summation of individual dynein forces, resulting in greatly increased average force production. This is consistent with theoretical studies indicating that force-detachment kinetics affect ensemble motor function (Kunwar et al., 2008). Nuclear oscillatory movements in *S. pombe* have been estimated to require ~50 dyneins (Vogel et al., 2009), many more than the 3–5 molecules reported for small membranous organelles (Shubeita et al., 2008; Soppina et al., 2009). Our test for LIS1-NudE stimulation of multimotor transport showed a dramatic increase in the ability to escape from an optical trap under high force conditions. These results reveal that, although individual dynein molecules are stalled under load in the presence of LIS1 and NudE, additional dynein-LIS1-NudE complexes strongly enhance the ability to move along microtubules under opposing loads. In silico modeling yielded virtually identical results (Figure 6B and Figure S5). We believe our results, therefore, explain the role of LIS1 in nuclear movement and likely in several additional cellular functions, including transport of large arrays of microtubules in radially migrating neurons and other cell types, mitotic spindle orientation, and aspects of chromosome movement. In contrast, we have found that small vesicular dynein cargoes showed no change in subcellular distribution in cells expressing LIS1 dominant-negative cDNA (Faulkner et al., 2000), and dynein-transported virus particles showed no detectable sensitivity to LIS1 inhibition (Bremner et al., 2009). Whether LIS1, nonetheless, could have some role in low load functions remains to be investigated more fully.

NudE and NudEL have been found to recruit dynein to kinetochores (Liang et al., 2007; Stehman et al., 2007; Vergnolle and Taylor, 2007), centrosomes (Guo et al., 2006), and possibly other structures. Therefore, we propose that these proteins target dynein and LIS1 to specific subcellular sites and, together with LIS1, control dynein force production as required. NudE and NudEL may have the additional function of silencing dynein at these sites until LIS1 is available, as suggested by the effects of NudE on single dynein molecules in the current assays.

EXPERIMENTAL PROCEDURES

Protein Purification

Bovine or rat brain cytoplasmic dynein, baculovirus-expressed dynein motor domain, and recombinant NudE were purified as described (Hook et al., 2005; Paschal et al., 1987; Stehman et al., 2007), except that the GST tag was removed from the NudE by PreScission protease cleavage (GE Biosciences). African green monkey LIS1 (Faulkner et al., 2000) was cloned into the Bac-N-Blue baculovirus system (Invitrogen) with an N-terminal His_6-tag and expressed according to the manufacturer's protocols. Recombinant kinesin (K560, Addgene- Cambridge, MA, USA) was expressed and purified using standard procedures.

Immunoprecipitations

Immunoprecipitation was performed using streptavidin beads (Invitrogen) incubated with a biotinylated monoclonal anti-His_6 antibody (QIAGEN) and then incubated with His_6-tagged LIS1 for 1 hr on ice. The beads were then mixed with NudE and/or dynein at 4°C for 1 hr in Tris-KCl buffer. Beads were then washed five times with buffer and samples were processed for western blot analysis using a LI-COR Odyssey imaging system.

Microtubule Binding

To assay effects of LIS1 and NudE on dynein microtubule binding, the proteins were mixed together at a 1:10 (Dyn:LIS1/NudE) ratio and incubated with 1 mg/ml final concentration of taxol-stabilized microtubules (Cytoskeleton, Inc.) and indicated nucleotides for 10 min at 37°C. ATP concentration was 10 mM with or without equimolar VO_4.

Bead Assays

Bead assays, including force measurements, and video recording and analysis of bead motion were performed essentially as previously described (Mallik et al., 2004; Vershinin et al., 2007) (for small exceptions, see Extended Experimental Procedures). Protein adsorption on beads was done via sequential incubations (10 min at room temperature) with motors, blocking agent (5.5 mg/ml casein), and dynein cofactors (LIS1 and NudE). Cofactors were removed by centrifugation in the "washed" assays and were left in solution in the "unwashed" assays. For data in Figure 4B (D Ab), the antibody was first nonspecifically adsorbed on beads followed by casein blocking and incubation with dynein (buffer exchanged at each step).

Superstall Experiments

Beads driven by a single dynein motor were subjected to ~2 pN of force (superstall condition) via a rapid change in optical trap stiffness. The duration of a superstall event was identified as the subsequent time for bead position to return to trap center.

Multiple-Motor Escape Experiments

Beads incubated with identical amounts of dynein in the presence or absence of NudE and LIS1 (parallel assays) were tested for ability to escape a trap of fixed stiffness. The fraction of escaped D and DNL beads was determined for two different dynein concentrations (and thus different mean number of engaged motors). Trap stiffness was different for each motor concentration.

Detailed methods can be found in the Extended Experimental Procedures.

SUPPLEMENTAL INFORMATION

Supplemental Information includes Extended Experimental Procedures and five figures and can be found with this article online at doi:10.1016/j.cell.2010.02.035.

ACKNOWLEDGMENTS

We acknowledge Drs. Jing Xu, Silvia Cermelli, and Peter Hook for helpful discussions and Shahrnaz Kemal, Kassandra Ori-McKenney, and Z. Shu for technical help. This work was supported by grants GM47434 and HD40182 to R.B.V. and grants 1RO1GM070676 and GM079156 to S.P.G. A.K. was supported by grant GM068952.

Received: May 18, 2009
Revised: December 18, 2009
Accepted: February 18, 2010
Published: April 15, 2010

REFERENCES

Bremner, K.H., Scherer, J., Yi, J., Vershinin, M., Gross, S.P., and Vallee, R.B. (2009). Adenovirus transport via direct interaction of cytoplasmic dynein with the viral capsid hexon subunit. Cell Host Microbe *6*, 523–535.

Burgess, S.A., Walker, M.L., Sakakibara, H., Knight, P.J., and Oiwa, K. (2003). Dynein structure and power stroke. Nature *421*, 715–718.

Chen, B., Doucleff, M., Wemmer, D.E., De Carlo, S., Huang, H.H., Nogales, E., Hoover, T.R., Kondrashkina, E., Guo, L., and Nixon, B.T. (2007). ATP ground- and transition states of bacterial enhancer binding AAA+ ATPases support complex formation with their target protein, sigma54. Structure *15*, 429–440.

Coquelle, F.M., Caspi, M., Cordelieres, F.P., Dompierre, J.P., Dujardin, D.L., Koifman, C., Martin, P., Hoogenraad, C.C., Akhmanova, A., Galjart, N., et al. (2002). LIS1, CLIP-170's key to the dynein/dynactin pathway. Mol. Cell. Biol. *22*, 3089–3102.

Derewenda, U., Tarricone, C., Choi, W.C., Cooper, D.R., Lukasik, S., Perrina, F., Tripathy, A., Kim, M.H., Cafiso, D.S., Musacchio, A., and Derewenda, Z.S. (2007). The structure of the coiled-coil domain of Ndel1 and the basis of its interaction with Lis1, the causal protein of Miller-Dieker lissencephaly. Structure *15*, 1467–1481.

Dietrich, K.A., Sindelar, C.V., Brewer, P.D., Downing, K.H., Cremo, C.R., and Rice, S.E. (2008). The kinesin-1 motor protein is regulated by a direct interaction of its head and tail. Proc. Natl. Acad. Sci. USA *105*, 8938–8943.

Dobyns, W.B. (1987). Developmental aspects of lissencephaly and the lissencephaly syndromes. Birth Defects *23*, 225–241.

Dujardin, D.L., Barnhart, L.E., Stehman, S.A., Gomes, E.R., Gundersen, G.G., and Vallee, R.B. (2003). A role for cytoplasmic dynein and LIS1 in directed cell movement. J. Cell Biol. *163*, 1205–1211.

Efimov, V.P., and Morris, N.R. (2000). The LIS1-related NUDF protein of Aspergillus nidulans interacts with the coiled-coil domain of the NUDE/RO11 protein. J. Cell Biol. *150*, 681–688.

Evans, E. (2001). Probing the relation between force–lifetime–and chemistry in single molecular bonds. Annu. Rev. Biophys. Biomol. Struct. *30*, 105–128.

Faulkner, N.E., Dujardin, D.L., Tai, C.Y., Vaughan, K.T., O'Connell, C.B., Wang, Y., and Vallee, R.B. (2000). A role for the lissencephaly gene LIS1 in mitosis and cytoplasmic dynein function. Nat. Cell Biol. *2*, 784–791.

Feng, Y., Olson, E.C., Stukenberg, P.T., Flanagan, L.A., Kirschner, M.W., and Walsh, C.A. (2000). LIS1 regulates CNS lamination by interacting with mNudE, a central component of the centrosome. Neuron *28*, 665–679.

Gebhardt, J.C., Clemen, A.E., Jaud, J., and Rief, M. (2006). Myosin-V is a mechanical ratchet. Proc. Natl. Acad. Sci. USA *103*, 8680–8685.

Gennerich, A., Carter, A.P., Reck-Peterson, S.L., and Vale, R.D. (2007). Force-induced bidirectional stepping of cytoplasmic dynein. Cell *131*, 952–965.

Grabham, P.W., Seale, G.E., Bennecib, M., Goldberg, D.J., and Vallee, R.B. (2007). Cytoplasmic dynein and LIS1 are required for microtubule advance during growth cone remodeling and fast axonal outgrowth. J. Neurosci. *27*, 5823–5834.

Guo, J., Yang, Z., Song, W., Chen, Q., Wang, F., Zhang, Q., and Zhu, X. (2006). Nudel contributes to microtubule anchoring at the mother centriole and is involved in both dynein-dependent and -independent centrosomal protein assembly. Mol. Biol. Cell *17*, 680–689.

Han, G., Liu, B., Zhang, J., Zuo, W., Morris, N.R., and Xiang, X. (2001). The Aspergillus cytoplasmic dynein heavy chain and NUDF localize to microtubule ends and affect microtubule dynamics. Curr. Biol. *11*, 719–724.

Hirotsune, S., Fleck, M.W., Gambello, M.J., Bix, G.J., Chen, A., Clark, G.D., Ledbetter, D.H., McBain, C.J., and Wynshaw-Boris, A. (1998). Graded reduction of *Pafah1b1 (Lis1)* activity results in neuronal migration defects and early embryonic lethality. Nat. Genet. *19*, 333–339.

Hook, P., Mikami, A., Shafer, B., Chait, B.T., Rosenfeld, S.S., and Vallee, R.B. (2005). Long range allosteric control of cytoplasmic dynein ATPase activity by the stalk and C-terminal domains. J. Biol. Chem. *280*, 33045–33054.

Imamula, K., Kon, T., Ohkura, R., and Sutoh, K. (2007). The coordination of cyclic microtubule association/dissociation and tail swing of cytoplasmic dynein. Proc. Natl. Acad. Sci. USA *104*, 16134–16139.

King, S.J., and Schroer, T.A. (2000). Dynactin increases the processivity of the cytoplasmic dynein motor. Nat. Cell Biol. *2*, 20–24.

Kon, T., Imamula, K., Roberts, A.J., Ohkura, R., Knight, P.J., Gibbons, I.R., Burgess, S.A., and Sutoh, K. (2009). Helix sliding in the stalk coiled coil of dynein couples ATPase and microtubule binding. Nat. Struct. Mol. Biol. *16*, 325–333.

Kon, T., Nishiura, M., Ohkura, R., Toyoshima, Y.Y., and Sutoh, K. (2004). Distinct functions of nucleotide-binding/hydrolysis sites in the four AAA modules of cytoplasmic dynein. Biochemistry *43*, 11266–11274.

Krementsov, D.N., Krementsova, E.B., and Trybus, K.M. (2004). Myosin V: regulation by calcium, calmodulin, and the tail domain. J. Cell Biol. *164*, 877–886.

Kunwar, A., Vershinin, M., Xu, J., and Gross, S.P. (2008). Stepping, strain gating, and an unexpected force-velocity curve for multiple-motor-based transport. Curr. Biol. *18*, 1173–1183.

Liang, Y., Yu, W., Li, Y., Yang, Z., Yan, X., Huang, Q., and Zhu, X. (2004). Nudel functions in membrane traffic mainly through association with Lis1 and cytoplasmic dynein. J. Cell Biol. *164*, 557–566.

Liang, Y., Yu, W., Li, Y., Yu, L., Zhang, Q., Wang, F., Yang, Z., Du, J., Huang, Q., Yao, X., and Zhu, X. (2007). Nudel modulates kinetochore association and function of cytoplasmic dynein in M phase. Mol. Biol. Cell *18*, 2656–2666.

Mallik, R., Carter, B.C., Lex, S.A., King, S.J., and Gross, S.P. (2004). Cytoplasmic dynein functions as a gear in response to load. Nature *427*, 649–652.

Mallik, R., Petrov, D., Lex, S.A., King, S.J., and Gross, S.P. (2005). Building complexity: an in vitro study of cytoplasmic dynein with in vivo implications. Curr. Biol. *15*, 2075–2085.

Mesngon, M.T., Tarricone, C., Hebbar, S., Guillotte, A.M., Schmitt, E.W., Lanier, L., Musacchio, A., King, S.J., and Smith, D.S. (2006). Regulation of cytoplasmic dynein ATPase by Lis1. J. Neurosci. *26*, 2132–2139.

Niethammer, M., Smith, D.S., Ayala, R., Peng, J., Ko, J., Lee, M.S., Morabito, M., and Tsai, L.H. (2000). NUDEL is a novel Cdk5 substrate that associates with LIS1 and cytoplasmic dynein. Neuron *28*, 697–711.

Paschal, B.M., and Vallee, R.B. (1987). Retrograde transport by the microtubule associated protein MAP 1C. Nature *330*, 181–183.

Paschal, B.M., Shpetner, H.S., and Vallee, R.B. (1987). MAP 1C is a microtubule-activated ATPase which translocates microtubules *in vitro* and has dynein-like properties. J. Cell Biol. *105*, 1273–1282.

Reck-Peterson, S.L., Yildiz, A., Carter, A.P., Gennerich, A., Zhang, N., and Vale, R.D. (2006). Single-molecule analysis of Dynein processivity and stepping behavior. Cell *126*, 335–348.

Reiner, O., Carrozzo, R., Shen, Y., Wehnert, M., Faustinella, F., Dobyns, W.B., Caskey, C.T., and Ledbetter, D.H. (1993). Isolation of a Miller-Dieker lissencephaly gene containing G protein β-subunit-like repeats. Nature *364*, 717–721.

Ross, J.L., Wallace, K., Shuman, H., Goldman, Y.E., and Holzbaur, E.L. (2006). Processive bidirectional motion of dynein-dynactin complexes in vitro. Nat. Cell Biol. *8*, 562–570.

Sapir, T., Elbaum, M., and Reiner, O. (1997). Reduction of microtubule catastrophe events by LIS1, platelet-activating factor acetylhydrolase subunit. EMBO J. *16*, 6977–6984.

Sasaki, S., Shionoya, A., Ishida, M., Gambello, M.J., Yingling, J., Wynshaw-Boris, A., and Hirotsune, S. (2000). A LIS1/NUDEL/cytoplasmic dynein heavy chain complex in the developing and adult nervous system. Neuron *28*, 681–696.

Scholey, J.M., Taylor, K.A., and Kendrick-Jones, J. (1980). Regulation of non-muscle myosin assembly by calmodulin-dependent light chain kinase. Nature *287*, 233–235.

Schroeder, H.W., Shuman, H., Holzbaur, E.L., and Goldman, Y.F. (2008). Cargo switching at actin-microtubule intersections: a case for strength in numbers. Mol. Biol. Cell *19* (suppl.), 325/B269.

Shen, Y., Li, N., Wu, S., Zhou, Y., Shan, Y., Zhang, Q., Ding, C., Yuan, Q., Zhao, F., Zeng, R., and Zhu, X. (2008). Nudel binds Cdc42GAP to modulate Cdc42 activity at the leading edge of migrating cells. Dev. Cell *14*, 342–353.

Shimizu, T., and Johnson, K.A. (1983). Kinetic evidence for multiple dynein ATPase sites. J. Biol. Chem. *258*, 13841–13846.

Shu, T., Ayala, R., Nguyen, M.D., Xie, Z., Gleeson, J.G., and Tsai, L.H. (2004). Ndel1 operates in a common pathway with LIS1 and cytoplasmic dynein to regulate cortical neuronal positioning. Neuron *44*, 263–277.

Shubeita, G.T., Tran, S.L., Xu, J., Vershinin, M., Cermelli, S., Cotton, S.L., Welte, M.A., and Gross, S.P. (2008). Consequences of motor copy number on the intracellular transport of kinesin-1-driven lipid droplets. Cell *135*, 1098–1107.

Siller, K.H., Serr, M., Steward, R., Hays, T.S., and Doe, C.Q. (2005). Live imaging of Drosophila brain neuroblasts reveals a role for Lis1/dynactin in spindle assembly and mitotic checkpoint control. Mol. Biol. Cell *16*, 5127–5140.

Smith, D.S., Niethammer, M., Ayala, R., Zhou, Y., Gambello, M.J., Wynshaw-Boris, A., and Tsai, L.H. (2000). Regulation of cytoplasmic dynein behaviour and microtubule organization by mammalian Lis1. Nat. Cell Biol. *2*, 767–775.

Soppina, V., Rai, A.K., Ramaiya, A.J., Barak, P., and Mallik, R. (2009). Tug-of-war between dissimilar teams of microtubule motors regulates transport and fission of endosomes. Proc. Natl. Acad. Sci. USA *106*, 19381–19386.

Stehman, S.A., Chen, Y., McKenney, R.J., and Vallee, R.B. (2007). NudE and NudEL are required for mitotic progression and are involved in dynein recruitment to kinetochores. J. Cell Biol. *178*, 583–594.

Stock, M.F., Guerrero, J., Cobb, B., Eggers, C.T., Huang, T.G., Li, X., and Hackney, D.D. (1999). Formation of the compact confomer of kinesin requires a COOH-terminal heavy chain domain and inhibits microtubule-stimulated ATPase activity. J. Biol. Chem. *274*, 14617–14623.

Svoboda, K., and Block, S.M. (1994). Force and velocity measured for single kinesin molecules. Cell *77*, 773–784.

Tai, C.Y., Dujardin, D.L., Faulkner, N.E., and Vallee, R.B. (2002). Role of dynein, dynactin, and CLIP-170 interactions in LIS1 kinetochore function. J. Cell Biol. *156*, 959–968.

Tarricone, C., Perrina, F., Monzani, S., Massimiliano, L., Kim, M.H., Derewenda, Z.S., Knapp, S., Tsai, L.H., and Musacchio, A. (2004). Coupling PAF signaling to dynein regulation: Structure of LIS1 in complex with PAF-acetylhydrolase. Neuron *44*, 809–821.

Toba, S., Watanabe, T.M., Yamaguchi-Okimoto, L., Toyoshima, Y.Y., and Higuchi, H. (2006). Overlapping hand-over-hand mechanism of single molecular motility of cytoplasmic dynein. Proc. Natl. Acad. Sci. USA *103*, 5741–5745.

Tsai, J.W., Chen, Y., Kriegstein, A.R., and Vallee, R.B. (2005). LIS1 RNA interference blocks neural stem cell division, morphogenesis, and motility at multiple stages. J. Cell Biol. *170*, 935–945.

Tsai, J.W., Bremner, K.H., and Vallee, R.B. (2007). Dual subcellular roles for LIS1 and dynein in radial neuronal migration in live brain tissue. Nat. Neurosci. *10*, 970–979.

Veigel, C., Schmitz, S., Wang, F., and Sellers, J.R. (2005). Load-dependent kinetics of myosin-V can explain its high processivity. Nat. Cell Biol. *7*, 861–869.

Vergnolle, M.A., and Taylor, S.S. (2007). Cenp-F links kinetochores to Ndel1/Nde1/Lis1/dynein microtubule motor complexes. Curr. Biol. *17*, 1173–1179.

Vershinin, M., Carter, B.C., Razafsky, D.S., King, S.J., and Gross, S.P. (2007). Multiple-motor based transport and its regulation by Tau. Proc. Natl. Acad. Sci. USA *104*, 87–92.

Vershinin, M., Xu, J., Razafsky, D.S., King, S.J., and Gross, S.P. (2008). Tuning microtubule-based transport through filamentous MAPs: the problem of dynein. Traffic *9*, 882–892.

Vogel, S.K., Pavin, N., Maghelli, N., Julicher, F., and Tolic-Norrelykke, I.M. (2009). Self-organization of dynein motors generates meiotic nuclear oscillations. PLoS Biol. *7*, e1000087.

Wang, F., Thirumurugan, K., Stafford, W.F., Hammer, J.A., 3rd, Knight, P.J., and Sellers, J.R. (2004). Regulated conformation of myosin V. J. Biol. Chem. *279*, 2333–2336.

Xiang, X., Osmani, A.H., Osmani, S.A., Xin, M., and Morris, N.R. (1995). NudF, a nuclear migration gene in Aspergillus nidulans, is similar to the human LIS-1 gene required for neuronal migration. Mol. Biol. Cell *6*, 297–310.

Yamada, M., Toba, S., Yoshida, Y., Haratani, K., Mori, D., Yano, Y., Mimori-Kiyosue, Y., Nakamura, T., Itoh, K., Fushiki, S., et al. (2008). LIS1 and NDEL1 coordinate the plus-end-directed transport of cytoplasmic dynein. EMBO J. *27*, 2471–2483.

Yan, X., Li, F., Liang, Y., Shen, Y., Zhao, X., Huang, Q., and Zhu, X. (2003). Human Nudel and NudE as regulators of cytoplasmic dynein in poleward protein transport along the mitotic spindle. Mol. Cell. Biol. *23*, 1239–1250.

Cell

EXTENDED EXPERIMENTAL PROCEDURES

ATPase Assays

ATPase activity was assayed using the malachite green method (Hook et al., 2005) in Tris-KCl buffer (Paschal et al., 1987) and incubated at 37°C for 15 min in the presence of 1 mM ATP. For microtubule stimulation, taxol-stabilized microtubules were added to 1 mg/ml final concentration before the addition of ATP.

Immunoprecipitations

Immunoprecipitations in Figure 1B were performed similarly in Tris-KCL buffer (20 mM Tris pH 7.6, 50 mM KCl, 5 mM $MgSO_4$, 0.5 mM EDTA) except the purified LIS1 protein was immobilized onto Protein A beads (Invitrogen) using an anti-N-terminal LIS1 antibody (Faulkner et al., 2000).

Sucrose Density Gradient

For sucrose gradient analysis, purified dynein motor domain (800 nM) with or without purified LIS1 (1600 nM) and the indicated nucleotides were mixed together on ice for 1 hr. The mixture was loaded onto 11 ml linear 5%–20% sucrose density gradients in buffer (35 mM PIPES pH 7.2, 5 mM $MgSO_4$, 1 mM EDTA, 0.5 mM EGTA) containing the corresponding nucleotides and centrifuged at 32K rpm for 16 hr in a Beckman SW41Ti rotor. Fractions (800 μl) were collected and analyzed by gel electrophoresis and Coomassie brilliant blue staining.

Bead Assays

Bead assays were performed as previously described (Mallik et al., 2004), except that GTP and taxol were omitted from the assay buffer, and an oxygen scavenging system was used as previously described (Vershinin et al., 2007). Video recording and analysis of bead motion were performed as previously described (Carter et al., 2005; Vershinin et al., 2007). Force measurements were also carried out as previously described (Vershinin et al., 2007). The majority of assays were done at motor/bead incubation ratios such that 30% or fewer beads showed MT-binding activity (Vershinin et al., 2007), so that the function of single dynein motors was characterized.

Protein adsorption on beads was done via sequential incubations (10 min at room temperature). Dynein was first incubated with carboxylated polystyrene beads (Vershinin et al., 2007), and the beads were then washed via mild centrifugation and resuspended in casein-containing buffer. In assays intended to study complexes, we followed this preparation with one of two approaches (referred to in the main text as ''washed'' and ''unwashed'' assays). In the ''washed'' assays, after preparing the dynein beads, each additional protein (NudE and/or LIS1) was incubated with the beads, and each incubation was followed by mild centrifugation to remove the unattached component from solution. (Assays without such intermediate buffer exchanges were found to give similar results.) After all such incubations, a final wash was performed. This was then followed by resuspension in the assay buffer described above. The ''unwashed'' assays were prepared similarly; however, the components were not removed via centrifugation following incubations. In the experiments described here, the incubation order was dynein then NudE for DN assays, dynein then LIS1 for DL assays, and dynein then NudE then LIS1 for DNL assays.

We have also attached dynein to polystyrene beads via the 74.1 monoclonal Anti-DIC antibody (Millipore Bioscience Research Reagents, Temecula, CA, USA). In these assays, the mAb was first nonspecifically adsorbed on beads (~1:20 bead:antibody molar ratio at incubation). Upon incubation, the beads were pelleted via mild centrifugation and then resuspended in 5 mg/ml casein buffer. Upon incubation the beads were again pelleted via mild centrifugation and then resuspended and incubated in motility buffer containing dynein.

Multiple-Motor Escape Experiments

To test the effect of NudE and LIS1 on multiple dynein motors, we devised a new type of trap escape experiment. For a given dynein concentration, we first attached dynein to beads and blocked the beads with casein. An examination of force production records for beads held near a microtubule in an optical trap allowed us to determine the approximate motor number and to choose a laser power such that only a small fraction of the control dynein beads were able to exert enough force over a long enough period of time (sufficient to observe several prominent events; 30 s typical) to escape from the trap. Once the appropriate trap stiffness was set for a particular dynein concentration, we then performed parallel experiments on beads in the presence or absence of NudE and LIS1 and determined the fraction of beads to escape the trap. Two different dynein concentrations were used to change the mean number of engaged motors, and correspondingly we used two different trap stiffness conditions, 0.01 pN/nm and 0.02 pN/nm for the low and high dynein concentrations, respectively (maximum trap force ~1.8 and 3.7 pN).

Binding Frequency Analysis from Quadrant Photodiode Records

To compare binding frequency in dynein-only and dynein/NudE assays using the force production recordings (Figures 4A and 4B), we faced the limitation that the extremely short processivity of the dynein/NudE complex made it difficult to distinguish between bead motion due to motor activity and bead motion due to thermal noise. To address this difficulty, we developed the following data analysis algorithm:

(1) Data were median filtered using a 10 point window (5 ms), to eliminate spurious noise.

(2) Filtered data were normalized by the maximum displacement occurring in each record.

(3) The start of each binding event was determined to occur when the instantaneous bead displacement first exceeded a defined constant threshold.

(4) The end of each binding event was determined to occur when the instantaneous bead position decreased, so that it was within 2 standard deviations of the trap center, where the standard deviation refers to the extent of thermal noise and was extracted from each record.

(5) Once the record had been processed, and all the binding events identified, we counted the number of binding events and normalized this number by the time duration of each record, to extract the binding rate.

The normalization (rescaling) in step 2 was done so that the differences in bead travel between assays would not affect the binding frequency analysis. Note, however, that this rescaling effectively amplifies noise for low-travel assays such as our dynein/NudE assay, so that in these assays noise-driven displacements are more likely to be improperly scored as binding events. Therefore, the estimate of binding reduction due to NudE provides a lower bound, and so the actual reduction is likely to be stronger.

Classifying Different Types of Binding

From observing beads in the dynein-NudE assays, we realized there were significantly more binding and release events (with negligible actual travel) than there were actual bead displacements appearing to reflect motor-driven transport. We were interested in quantifying the number of both classes of events. The first class provided evidence that at least one motor was present and marginally functional on the bead. The second class is the events that, though short and rare, reflect clearly processive transport. The analysis above using the quadrant photodiode was both very sensitive and with very high temporal resolution, and thus able to identify both classes of events. In addition, however, we wanted to focus only on the second class of events. To do this, we used our video records of bead movements in the optical trap. This system predominantly did not "see" the first class of events because the data rate for video recording (NTSC: ~33 ms/frame) did not resolve fast events whose travel fell below ~50–60 nm, the level of thermal-driven positional noise. Thus, binding events identified from video records (as opposed to quadrant photo-diode records) reflected significant motor activity. We therefore used video identification of microtubule binding as a metric for looking at significant events (Figure 4C).

Superstall Experiments

A bead driven by a single dynein motor was allowed to move 100 nm from the center of a weak optical trap (k = 0.01 pN/nm). At this displacement, the motor was still not subjected to stall conditions. The position of the bead was evaluated in a sliding 10 ms window to reduce noise. Once the smoothed bead position exceeded 100 nm, the trap stiffness was automatically doubled via a custom software control system, and the motor was subjected to ~2 pN of force (the 10 ms smoothing window may have resulted in a slight uncertainty of the initial instantaneous superforce). Both bead position and laser power were simultaneously recorded so that the onset of superforce regime could be determined in subsequent analysis. The superstall event started when the laser power was increased (T = 0), and ended when the motor detached from the microtubule, identified as the time when the bead displacement from trap center fell to within thermal noise level (typically, a sharp drop in bead position). Custom Matlab (Mathworks, Natick, MA, USA) and LabView (National Instruments, Austin, TX, USA) software were used for data recording and analysis.

Theoretical Model for Dynein-Based Motility

We assume that the dependence of the velocity v on applied load F can be well approximated for a single dynein motor by the following relation:

$$v(F) = v\left(1 - \left(\frac{F}{F_S}\right)^w\right) \tag{1}$$

where v is the unloaded velocity of dynein motor, F is the applied force, and F_s is the stall force. We chose w = 0.25 to model predicted sub- linear force-velocity relationship of dynein motor (Singh et al., 2005). Other force-velocity relationships including super-linear ones were investigated (results not shown) and were found to produce qualitatively similar results (enhancement of multiple-motor ensemble performance under load).

For motor's step size d, load-dependent rate of forward stepping is given by

$$k_{step\rightarrow}(F) = \begin{cases} \frac{v}{d}\left(1 - \left(\frac{F}{F_S}\right)^w\right) & F \le F_S \\ 0 & F > F_S \end{cases} \tag{2}$$

A forward load is assumed to not alter the motor cycle, so F = 0 for forward loads in Equation 2.

Following Klumpp and Lipowsky (2005), we use the Kramers's theory formula for the rate of motor detachment under backward load F,

$$\varepsilon(F) = \varepsilon \exp\left(\frac{F}{F_d}\right), \tag{3}$$

and we assume similar dynamics for back-stepping probability of dynein,

$$k_{step\leftarrow}(F) = \frac{\nu}{Bd}\exp\left(\frac{F}{F_d}\right) \tag{4}$$

where the scaling factor B is set to assure that the probability of back-stepping under no load is small relative to the probability of forward-stepping (here B = 40 which translates into a 2.5% rate of back-stepping under no load).

In the presence of the viscous load, position of the cargo is determined by the external load applied by the trap, forces exerted by motors on the bead as well as thermal noise. If a spherical bead of radius r immersed in a medium of dynamic viscosity η were subject to a net force *f* then (per Stokes' law) this would cause the bead to move with velocity $v_{drift} = (f/6\pi\eta r)$. Note that our simulations use the effective viscosity of water near the surface which is higher than bulk viscosity as per Faxen's law. Our simulations are not very sensitive to this scaling and similar qualitative results were seen for viscosities between 1e-3 $N\,s/m^2$ and 3e-3 $N\,s/m^2$.

To calculate the net motion of the bead over time interval Δt we superimpose the deterministic drift $x_{drift} = v_{drift}.\Delta t = (f/6\pi\eta r)\Delta t$ on the Brownian displacements x_{random} which are modeled as a random variable drawn from a normal distribution with mean square displacement $2D\Delta t$ (Beausang et al., 2007; Kunwar et al., 2008; Mogilner et al., 2002). Here D is the diffusion constant of the bead (thermal displacements of the motors are assumed to be negligible).

To summarize, the bead displacement at time t and $t+\Delta t$ are related by:

$$\vec{x}(t+\Delta t) = \vec{x}(t) + \vec{x}_{random} + \vec{x}_{drift} = \vec{x}(t) + \vec{x}_{random} + \frac{\vec{f}}{6\pi\eta r}(\Delta t). \tag{5}$$

The net force *f* on the bead is given by

$$\vec{f} = \vec{F} + \sum_{i=1}^{n} f_i$$

where F is the external force on the bead whose magnitude depends on the displacement of the bead from the trap center $F = k_{trap}(x\text{-}x_{trap})$. Note that an engaged dynein motor forms a linkage between the cargo and the microtubule with rest length 50 nm and stiffness 0.32 pN/nm. In our model, the i^{th} motor exerts a restoring force $f_i = k\Delta l_i$ when it is stretched by Δl_i beyond its rest length and has no compressional rigidity, i.e., it exerts no force when compressed.

Simulation Algorithm

For each time step, we visit each of the N motors and determine their tentative states (attached or detached) and positions. If a motor is currently unattached, we give it a chance to attach with a probability determined by the assumed "on-rate" (P_{on}). If a motor is currently attached, there are four possibilities: it can remain stationary, take a forward step, take a backward step, or detach. To determine what the motor does, we first calculate the force it experiences taking into account that the force felt by a given motor depends on its position relative to the position of the bead. Once the load on a motor is determined, we then test if it steps, remains stationary, or detaches, where the probability of each event is determined from the single-motor model (see above). When we have determined the tentative states and positions of all N motors, we update the states and positions of all motors simultaneously. Finally, we calculate the new position of the bead using the new motor states and positions (Equation 5). We then record the positions and states of all motors and the overall location of the cargo.

In our simulations, a cargo carries N motors (which is the upper limit on the number of instantaneously engaged motors n). The update procedure for each configuration is detailed below.

Algorithm in Detail

We denote the current position of the cargo by x, the current time by t, and the current number of engaged motors by n. To start with the initial condition of single motor attached, we place the bead's center of mass at the center of the trap x_{trap} on the track. The motor is allowed to attach to any discrete binding site on the track within distance l on either side of the bead's center of mass. Thus, at t = 0, $x = x_{trap}$, and n = 1. We update the state of the model in steps of Δt up to time t_{max}. Every motor is updated once and only once in a given time step.

For each time step, if $t > t_{max}$, then terminate further simulation, otherwise for each motor, we follow the update algorithm below:

(a) Update the motor state:

A1. *Updating a detached motor:* Examine every motor on the cargo. If a given motor is in a detached state, it gets an opportunity to attach with probability $P_{on} = \pi\Delta t$ to any binding site on the track within distance l on either side from the center of mass of the bead. The probability of binding to the track is modeled as a truncated Gaussian with width (HWHM) equal to half motor length (25 nm). We have also tested uniform binding probability model and seen qualitatively similar results.

A2. *Updating an attached motor*: Examine every motor on the cargo not already updated in step A1. If a given motor is engaged then:

B1. Test for detachment with probability given by Equation 3. If detachment occurs then go to step B3.

B2. Test for forward stepping with a probability given by Equation 2 or back stepping with a probability given by Equation 4. The test is designed to be mutually exclusive so that only one outcome can occur per time step. If a step occurs then x_i is incremented to $x_i + d$ for a forward step or $x_i - d$ for a backward step.

B3. Proceed to update the next motor or step (b) if all motors are updated.

(b) Calculate n (the number of instantaneously engaged motors): if n = 0, then record the final position of the bead $x_{final} = x$, and end the simulation, else update the cargo position as per Equation 5 and proceed to simulating the next time step.

Parameter Values for Simulations

The parameter values used are v = 1 μm/s, d = 8 nm, $\varepsilon = 1\ s^{-1}$, $F_s = 1.5$ pN and $F_d = 0.87$ pN, 1.055 pN, and 2.89 pN as indicated, l = 50 nm, k = 0.01pN/nm (low number of motors in Figure 6B) and 0.02 pN/nm nm (high number of motors in Figure 6B), r = 0.25 μm. In each case, Monte Carlo results were obtained from runs each having a duration of $t_{max} = 100$ s (1 time step = 10^{-7}s).

Our model assumes that all N motors are clustered at one spot on the cargo however in reality motors likely bind randomly on the surface of the bead. We expect that motors that bind away from the microtubule-facing spot on the bead will have lower on-rate and we have attempted to take such geometric factors of motor binding into account when modeling beads with high versus low motor density (N = 1, 2, and 4). Thus, for low motor density we assumed $\pi = 0.4\ s^{-1}$ and for high motor density $\pi = 4\ s^{-1}$. The simulations shown in Figure 6 for the low trap stiffness case had 20% of beads with N = 2 and 80% with N = 1. In the high trap stiffness case, N = 4 was used for all beads.

For trap escape modeling in Figure 6B, each run was simulated as described above and then all runs (total runs = 10000) were split into non-overlapping groups of 20 to account for the fact that in the in vitro experiments each bead was given multiple chances to escape from the trap (20 attempts typical). Failure of trap escape for each group was recorded if none of the runs in the group resulted in an escape.

Reporting Error Bars for Binomial-Distributed Data

It is common to report standard error of the mean (or standard deviation) as an error bar estimate for Gaussian distributed variables. However, a binomial distribution is in many cases poorly approximated by a normal distribution. We have therefore used a conceptually similar error estimate: 68.2689% exact CI for a binomial distribution for all data which is expected to have a binomial distribution (Figures 3B, 4D, and 6B and Figure S2). A Bayesian estimation with uniform prior distribution yielded similar values.

SUPPLEMENTAL REFERENCES

Beausang, J.F., Zurla, C., Finzi, L., Sullivan, L., and Nelson, P.C. (2007). Elementary simulation of tethered Brownian motion. Am. J. Phys. *75*, 520–523.

Carter, B.C., Shubeita, G.T., and Gross, S.P. (2005). Tracking single particles: a user-friendly quantitative evaluation. Phys. Biol. *2*, 60–72.

Faulkner, N.E., Dujardin, D.L., Tai, C.Y., Vaughan, K.T., O'Connell, C.B., Wang, Y., and Vallee, R.B. (2000). A role for the lissencephaly gene LIS1 in mitosis and cytoplasmic dynein function. Nat. Cell Biol. *2*, 784–791.

Hook, P., Mikami, A., Shafer, B., Chait, B.T., Rosenfeld, S.S., and Vallee, R.B. (2005). Long range allosteric control of cytoplasmic dynein ATPase activity by the stalk and C-terminal domains. J. Biol. Chem. *280*, 33045–33054.

Klumpp, S., and Lipowsky, R. (2005). Cooperative cargo transport by several molecular motors. Proc. Natl. Acad. Sci. USA *102*, 17284–17289.

Kunwar, A., Vershinin, M., Xu, J., and Gross, S.P. (2008). Stepping, strain gating, and an unexpected force-velocity curve for multiple-motor-based transport. Curr. Biol. *18*, 1173–1183.

Mallik, R., Carter, B.C., Lex, S.A., King, S.J., and Gross, S.P. (2004). Cytoplasmic dynein functions as a gear in response to load. Nature *427*, 649–652.

Mogilner, A., Elston, T., Wang, H.Y., and Oster, G. (2002). Molecular motors: Theory. Joel Keizer's Computational Cell Biology, 321–355.

Paschal, B.M., Shpetner, H.S., and Vallee, R.B. (1987). MAP 1C is a microtubule-activated ATPase which translocates microtubules in vitro and has dynein-like properties. J. Cell Biol. *105*, 1273–1282.

Singh, M.P., Mallik, R., Gross, S.P., and Yu, C.C. (2005). Monte Carlo modeling of single-molecule cytoplasmic dynein. Proc. Natl. Acad. Sci. USA *102*, 12059–12064.

Vershinin, M., Carter, B.C., Razafsky, D.S., King, S.J., and Gross, S.P. (2007). Multiple-motor based transport and its regulation by Tau. Proc. Natl. Acad. Sci. USA *104*, 87–92.

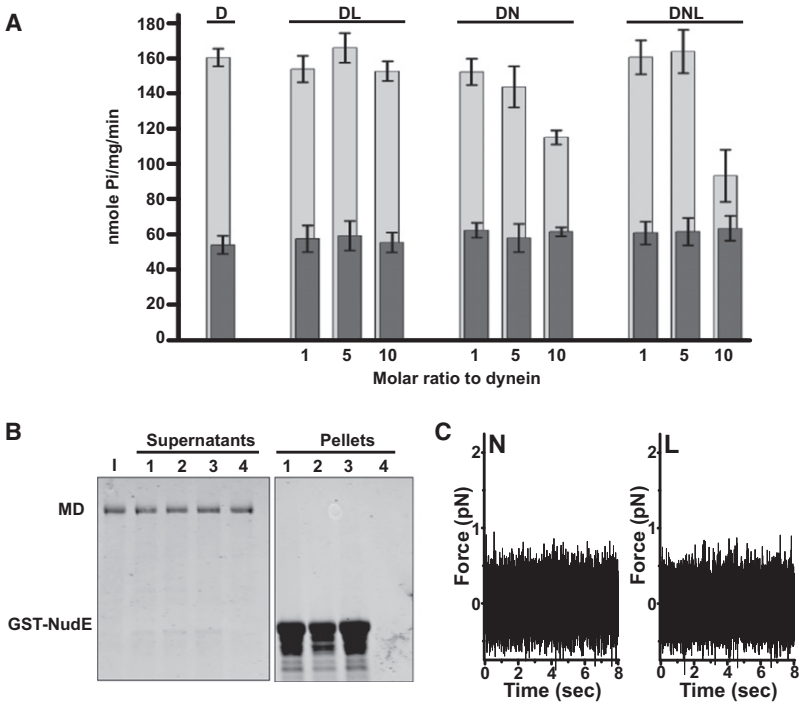

Figure S1. Effects of NudE and LIS1 on Microtubule Binding and ATPase Activity, Related to Figure 2

(A) Brain cytoplasmic dynein (D) was mixed with NudE (DN) and/or LIS1 (DL or DNL) with (light gray bars) or without microtubules (dark gray bars), and ATPase activity was determined. LIS1 and NudE had no effect on basal ATPase activity, but NudE alone and NudE plus LIS1 inhibited the microtubule-stimulated ATPase component. Error bars indicate standard deviation from three independent experiments.

(B) Pull-down of purified dynein motor domain with GST-tagged NudE as a function of nucleotide composition. No interaction was observed under conditions of no nucleotide (lane 1), ATP (lane 2), or ATP + VO_4 (lane 3). Input (I) and control beads (lane 4) are shown.

(C) NudE and LIS1 do not bind microtubules in the absence of dynein. Beads incubated with NudE alone (N), and LIS1 alone (L) were situated next to a microtubule in an optical trap and their position monitored. Systematic displacements of beads from the center of the trap (zero in all plots) would reveal individual motor events. Such events are nonexistent for (N) and (L). Nonspecific binding events should also be detectable in this assay, as evidenced by decreased noise in bead tracings in the absence of any systematic displacement of the beads. Such changes were not observed for N and L beads, arguing against nonspecific bead-MT binding. Moreover, these beads quickly diffused from the microtubules once the trap was turned off, further confirming the lack of any MT-binding activity in those assays.

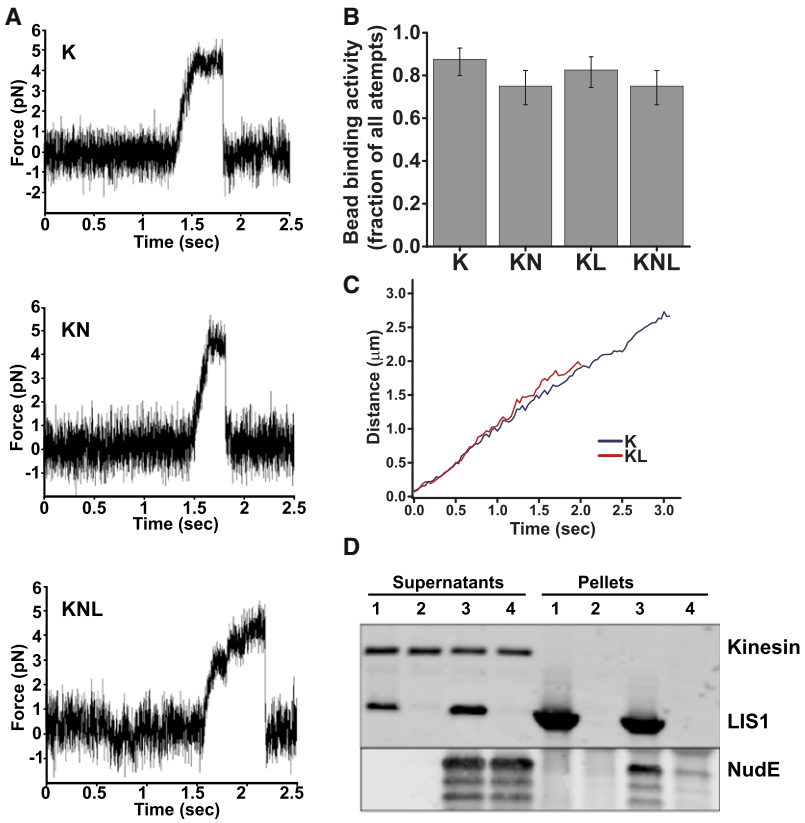

Figure S2. Lack of Effect of NudE and LIS1 on Kinesin Motility and Force Production, Related to Figure 3

(A) Representative records of single-motor force production in an optical trap are shown for beads adsorbed with a recombinant K560 kinesin construct alone (K), in the presence of NudE (KN; K:N 1:10), and in the presence of both NudE and LIS1 (KNL; K:N:L 1:10:10). Kinesin force production and stalling behavior under load were unaffected by LIS1 and NudE.

(B) Kinesin bead binding to MTs was minimally affected by the presence of NudE, LIS1, or both NudE and LIS1 (n = 40 in all cases, exact CI error bars are reported).

(C) Traces of processive motion along MTs for beads driven by kinesin alone (blue) and kinesin in the presence of 3X molar excess of LIS1 (red) reveal no pauses in motion. This is in contrast to frequent pauses seen for dynein motility in the presence of comparable levels of LIS1 (Figure 2B).

(D) Purified, recombinant kinesin (K560) does not interact with LIS1 (lane 1) or a LIS1-NudE complex (lane 3). No LIS1, NudE, or kinesin was pulled down by beads lacking LIS1 antibodies (lanes 2, 4).

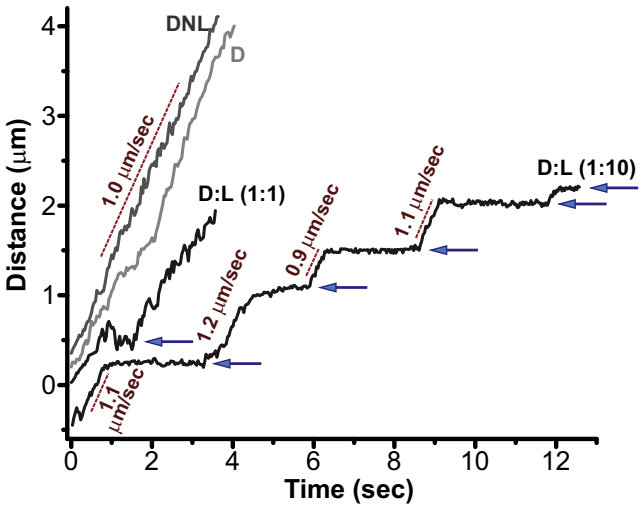

Figure S3. Additional Examples of D, DL, and DNL Motility, Related to Figure 3

Individual traces of motor-driven movements along microtubules (molar ratios were D:L = 1:10 and D:N:L = 1:9:10). DL bead movement is interrupted by unusually clear and frequent pauses (blue arrows), whereas D and DNL bead movement is prolonged and continuous.

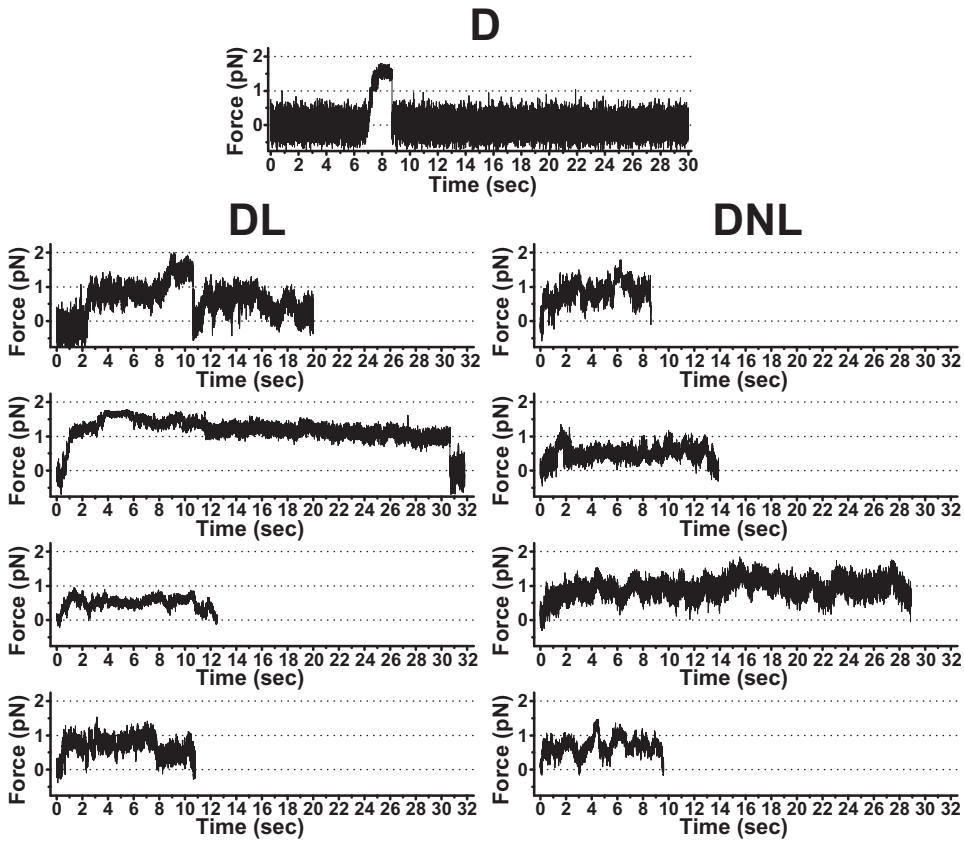

Figure S4. Additional Examples of LIS1 and NudE Effects on Dynein Force Production

Trace of dynein bead position in optical trap (D) is shown at top, including a longer force-producing event (~2 s), which is rare for dynein alone. Traces of dynein bead position are shown below in the presence of LIS1 (DL;1:10 D:L) or NudE plus LIS1 (DNL; 1:9:10 D:N:L; right panels) showing commonly observed persistent force events.

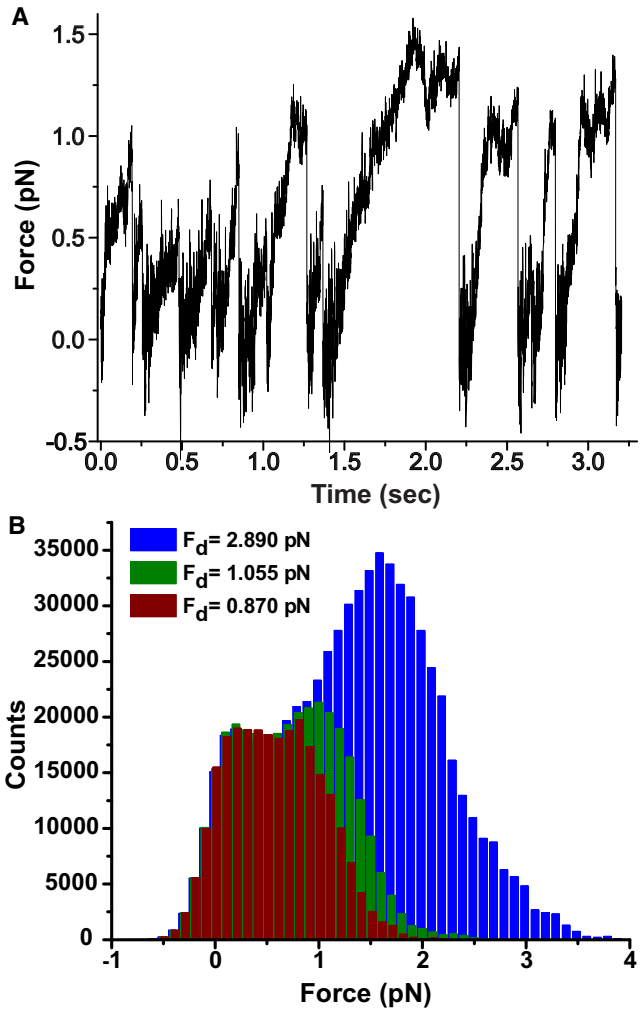

Figure S5. In Silico Modeling of Single and Multiple Dynein Activity, Related to Figure 6

(A) The model implemented in this paper is necessarily crude because many key parameters of cytoplasmic dynein function are not known. However, the model does capture important known observables, such as unloaded velocity, overall force production scale, and propensity to move bi-directionally rather than cleanly stall under load.

(B) We simulated motility of a cargo driven against a trap by a maximum of 2 motors (N = 2). The effect of the addition of NudE and LIS1 was modeled to decrease the detachment rate of the motors under load, such that at 2 pN the detachment time increased by 50% (and 500% for LIS1 alone), as suggested by the super-force experiments (Figure 5). This was implemented by varying detachment scale F_d such that an increase of F_d resulted in a corresponding increase for time to detachment under load (see Extended Experimental Procedures, section "Theoretical Model for Dynein-Based Motility"). The histograms of all predicted bead positions thus obtained (trap stiffness of 0.01 pN/nm) were calculated for 1000 simulations for baseline case, as well as 50% and 500% increase in time to detachment at 2 pN load (F_d of 0.87 pN [red], 1.055 pN [green], and 2.89 pN [blue], respectively). The predicted robust shift to higher values of force for the lower detachment rate case demonstrates that this parameter can have strong effect on multiple-motor performance. Notice also that the number of total counts rises as the detachment rate falls, directly implying that reduced detachment rate significantly enhances ensemble's ability to withstand load.